university of groningen

umcg

University of Groningen

A revised AMS and tephra chronology for the Late Middle to Early Upper Paleolithic occupations of Ortvale Klde, Republic of Georgia

Cullen, Victoria L.; Smith, Victoria C.; Tushabramishvili, Nicholaz; Mallol, Carolina; Dee, Michael; Wilkinson, Keith N.; Adler, Daniel S.

Published in:
Journal of Human Evolution

DOI:
10.1016/j.jhevol.2020.102908

IMPORTANT NOTE: You are advised to consult the publisher's version (publisher's PDF) if you wish to cite from it. Please check the document version below.

Document Version
Publisher's PDF, also known as Version of record

Publication date:
2021

Link to publication in University of Groningen/UMCG research database

Citation for published version (APA):
Cullen, V. L., Smith, V. C., Tushabramishvili, N., Mallol, C., Dee, M., Wilkinson, K. N., & Adler, D. S. (2021). A revised AMS and tephra chronology for the Late Middle to Early Upper Paleolithic occupations of Ortvale Klde, Republic of Georgia. *Journal of Human Evolution*, *151*, Article 102908. https://doi.org/10.1016/j.jhevol.2020.102908

Copyright
Other than for strictly personal use, it is not permitted to download or to forward/distribute the text or part of it without the consent of the author(s) and/or copyright holder(s), unless the work is under an open content license (like Creative Commons).

The publication may also be distributed here under the terms of Article 25fa of the Dutch Copyright Act, indicated by the "Taverne" license. More information can be found on the University of Groningen website: https://www.rug.nl/library/open-access/self-archiving-pure/taverne-amendment.

Take-down policy
If you believe that this document breaches copyright please contact us providing details, and we will remove access to the work immediately and investigate your claim.

Downloaded from the University of Groningen/UMCG research database (Pure): http://www.rug.nl/research/portal. For technical reasons the number of authors shown on this cover page is limited to 10 maximum.

Download date: 10-11-2026

Journal of Human Evolution 151 (2021) 102908

Contents lists available at ScienceDirect

Journal of Human Evolution

journal homepage: www.elsevier.com/locate/jhevol

A revised AMS and tephra chronology for the Late Middle to Early Upper Paleolithic occupations of Ortvale Klde, Republic of Georgia

Victoria L. Cullen [a, b], Victoria C. Smith [b], Nicholaz Tushabramishvili [c], Carolina Mallol [d, e], Michael Dee [f], Keith N. Wilkinson [g], Daniel S. Adler [h, *]

[a] Department of Chemistry, University of Oxford, Oxford, United Kingdom
[b] Research Laboratory for Archaeology and the History of Art, University of Oxford, Oxford, United Kingdom
[c] School of Engineering, Institute of Earth Sciences, Ilia State University, Tbilisi, Georgia
[d] Archaeological Micromorphology and Biomarker Research Lab, Instituto Universitario de Bio-Orgánica Antonio González, Tenerife, Spain
[e] Departamento de Geografía e Historia, Universidad de La Laguna Campus de Guajara, Tenerife, Spain
[f] Centre for Isotope Research, ESRIG, University of Groningen, Groningen, the Netherlands
[g] Department of Anthropology and Archaeology, University of Winchester, United Kingdom
[h] Department of Anthropology, University of Connecticut, CT, USA

ARTICLE INFO

Article history:
Received 13 January 2020
Accepted 26 October 2020

Keywords:
Late Middle Paleolithic
Early Upper Paleolithic
Southern Caucasus
Radiocarbon
Nemrut formation
Tephra

ABSTRACT

The nature and timing of the shift from the Late Middle Paleolithic (LMP) to the Early Upper Paleolithic (EUP) varied geographically, temporally, and substantively across the Near East and Eurasia; however, the result of this process was the archaeological disappearance of Middle Paleolithic technologies across the length and breadth of their geographic distribution. Ortvale Klde rockshelter (Republic of Georgia) contains the most detailed LMP-EUP archaeological sequence in the Caucasus, an environmentally and topographically diverse region situated between southwest Asia and Europe. Tephrochronological investigations at the site reveal volcanic ash (tephra) from various volcanic sources and provide a tephrostratigraphy for the site that will facilitate future correlations in the region. We correlate one of the cryptotephra layers to the large, caldera-forming Nemrut Formation eruption (30,000 years ago) from Nemrut volcano in Turkey. We integrate this tephrochronological constraint with new radiocarbon dates and published ages in an OxCal Bayesian age model to produce a revised chronology for the site. This model increases the ages for the end of the LMP (~47.5–44.2 ka cal BP) and appearance of the EUP (~46.7–43.6 ka cal BP) at Ortvale Klde, which are earlier than those currently reported for other sites in the Caucasus but similar to estimates for specific sites in southwest Asia and eastern Europe. These data, coupled with archaeological, stratigraphic, and taphonomic observations, suggest that at Ortvale Klde, (1) the appearance of EUP technologies of bone and stone has no technological roots in the preceding LMP, (2) a LMP population vacuum likely preceded the appearance of these EUP technologies, and (3) the systematic combination of tephra correlations and absolute dating chronologies promises to substantially improve our inter-regional understanding of this critical time interval of human evolution and the potential interconnectedness of hominins at different sites.

© 2020 Elsevier Ltd. All rights reserved.

1. Introduction

1.1. The shift from the Late Middle Paleolithic to Early Upper Paleolithic

The changes in lithic and organic technologies that define the shift from the Late Middle Paleolithic (LMP) to the Early Upper Paleolithic (EUP) are observed across Eurasia, albeit in varied forms and at different times. At some sites, compelling cases can be made for local technological continuity between the LMP and EUP (Mussi, 2001; Flas, 2011; Nigst, 2012; Ruebens, 2013; Hublin, 2015; Peresani et al., 2016), whereas at others, there are no clear precedents for the EUP assemblages that appear to replace previous LMP assemblages (Tostevin, 2000, 2012; Skrdla, 2003, 2017; Conard et al., 2006; Adler et al., 2006, 2008; Richter et al., 2008; Hoffecker, 2009; Rhodes et al., 2019; Fewlass et al., 2020). Recently, revised chronologies of sites in Western Europe suggest that LMP and EUP populations could have coexisted in some regions for millennia

* Corresponding author.
E-mail address: daniel.adler@uconn.edu (D.S. Adler).

https://doi.org/10.1016/j.jhevol.2020.102908
0047-2484/© 2020 Elsevier Ltd. All rights reserved.

(Higham et al., 2014; Fu et al., 2015), and chronological data show that the disappearance of the Neanderthals and other LMP populations was not temporally or geographically uniform, indicating a complex mosaic of interaction and change across Eurasia. Therefore, the regional and temporal variation in technology exhibited across the LMP-EUP boundary should be considered the norm rather than the exception, likely reflecting different trajectories in local cultural evolution and interactions, interpopulation connectivity, and population expansions, contractions, and extinctions rather than a single sweeping demographic change (Hovers, 2009; Barton and Riel-Salvatore, 2012; Kuhn, 2013; Higham et al., 2014; Stutz et al., 2015; Greenbaum et al., 2019a,b). While the social and demographic mechanisms underpinning the development and spread of EUP industries are rightly debated (Hovers and Belfer-Cohen, 2006; Teyssandier, 2008; d'Errico and Stringer, 2011; Villa and Roebroeks, 2014; Wynn et al., 2016; Greenbaum et al., 2019a,b), the appearance of the EUP in any given region appears to mark the end of the preceding LMP and represent a technological, behavioral, and perhaps biological tipping point from which there looks to have been no return for LMP populations, at least insofar as archaeologists currently define and recognize them in the absence of diagnostic fossil material or DNA.

Based on available chronometric data produced via different methods, the LMP-to-EUP shift occurred from ~50 to 40 ka across much of Eurasia (Higham et al., 2014; Nigst et al., 2014; Fewlass et al., 2020). While a small number of sites contain LMP assemblages associated with Neanderthal fossils (Hajdinjak et al., 2018) and an even smaller number of sites contain EUP assemblages associated with *Homo* sapiens (Hublin et al., 2020), the critical strata in the vast majority of sites contain no hominin fossil material whatsoever. This reality of the archaeological record, coupled with recent genetic data revealing multiple periods of *Homo sapiens* and Neanderthal admixture (Racimo et al., 2015; Kuhlwilm et al., 2016; Sankararaman et al., 2016; Vernot et al., 2016; Yang et al., 2017; Slon et al., 2018) and the interstratification and coexistence of different archaic hominins (e.g., Denisova Cave, Slon et al., 2017), requires a careful reassessment of longstanding assumptions about the use of lithic assemblages as proxies for hominin populations and/or species (see Clark and Riel-Salvatore, 2006; Shea, 2006; Hovers, 2009; Adler et al., 2014). In light of these ongoing developments in paleoanthropology, we remain agnostic as to the biological identity of the hominins occupying Ortvale Klde during any time interval and refer throughout the following pages to LMP and EUP hominins, populations, or technologies.

Much of the research on the timing of the LMP and EUP has focused on sites in Central and Western Europe, and substantially less is known about when this change and related changes occurred in Eastern Europe and in Central Asia (but see Fu et al., 2014; Douka et al., 2019; Jacobs et al., 2019; Fewlass et al., 2020). Revising the chronology of LMP and EUP sites in the Caucasus, an environmentally and topographically diverse region intermediate between Europe and Asia (Fig. 1), is crucial to our understanding of the development and expansion of EUP populations, their interactions with the LMP populations they encountered, and the archaeological demise of LMP technologies and perhaps their makers.

A series of recent excavations and dating programs at sites in the southern Caucasus have begun to refine our understanding of the LMP-EUP in terms of material culture, subsistence, mobility, and timing, the result being a consistent lack of transitional industries or evidence for in situ technological evolution (Adler et al., 2008; Golovanova et al., 2010b; Pinhasi et al., 2011, 2012; Tushabramishvili et al., 2012; Moncel et al., 2015; Pleurdeau et al., 2016; Douka and Higham, 2017). Furthermore, the ongoing sourcing of obsidian artifacts from several of these LMP and EUP sites is beginning to document the shifting scale of mobility during this and earlier time intervals (Adler et al., 2014; Frahm et al., 2016, 2019, 2020) and in the case of Ortvale Klde uncover nuanced evidence for increasing population interconnectivity and an expansion of the LMP social landscape (sensu Gamble, 1999) before and after the appearance of the EUP. Collectively, these data call into question the simplistic yet pervasive population replacement model.

Age estimates for the timing of the LMP-EUP across Eurasia, based primarily on radiocarbon dates, are highly variable from site to site, due in large part to the inconsistent application of ultrafiltration pretreatment methods, the difficulty of extracting adequate amounts of bone collagen for dating, which leads to inadequate sample sizes from layers and sites, and a widespread lack of detailed studies of site formation and taphonomy (e.g., micromorphology) with which to assess the stratigraphic and contextual integrity of dated samples and chronologies. Only by overcoming these limitations can an accurate and precise understanding of the LMP-EUP be achieved for this or any other region.

The most detailed LMP-EUP stratigraphic and archaeological sequence excavated in the southern Caucasus is found at Ortvale Klde in the Republic of Georgia (Fig. 1). The published chronology suggests that EUP technologies appear at Ortvale Klde between ~42 and 39 ka cal BP_{Hulu} (Adler et al., 2008), perhaps several millennia after they appeared elsewhere in Eurasia, leading to the hypothesis that the area served as a refugium for LMP hominins (Adler and Tushabramishvili, 2004). Since the full publication of the Ortvale Klde chronology, there have been a number of methodological advances in chronological approaches that include: (1) an improved 'ultrafiltration' method (UF) for bone pretreatment before radiocarbon dating, which can now more reliably remove degraded and contaminated fractions of organic material (e.g., Brock et al., 2016; Higham et al., 2011), (2) an updated radiocarbon calibration curve (IntCal20; Reimer et al., 2020) that extends the limit of the technique (ca. 55,000 yr cal BP) and takes into consideration the radiocarbon time dilation between 48 and 40 ka (Bard et al., 2020), and (3) the development of software packages such as OxCal (Bronk Ramsey, 1994, 2009a) that can generate Bayesian age models that integrate different types of chronological data, including relevant site stratigraphy, and calibrate radiocarbon ages to provide accurate and more precise age models (Buck et al., 1992). Tephrochronology, which uses volcanic ash layers (tephra) to obtain relative and absolute chronologies (e.g., using the Campanian Ignimbrite, see below), is now also being used to constrain chronologies and date archaeological sequences (e.g., Lowe et al., 2012). Here, we present the results of the first detailed cryptotephra research in the southern Caucasus, which provides a basis for further studies.

In the remaining sections of this article, we report how we have used recent methodological advances in radiocarbon dating and tephrochronology to further constrain the age of the Ortvale Klde sequence. We identify tephra layers in the sequence, present new radiocarbon dates on UF pretreated material, calibrate all radiocarbon data using IntCal20, and integrate these data with published age data (e.g., Adler et al., 2008, Table 1) in OxCal. The model provides more accurate and precise ages for the LMP and EUP at Ortvale Klde, extends the LMP-EUP back several thousand years, and allows us to test several hypotheses with regard to technological trends in the southern Caucasus.

1.2. A new approach to constraining the chronology of Ortvale Klde

Tephrochronology has only been used in the Caucasus at Mezmaiskaya Cave in southern Russia (Golovanova et al., 2010a) and Aghitu-3 in Armenia (Kandel et al., 2017). These two studies highlight the limited application but significant potential of detailed tephrostratigraphy in the Caucasus and, therefore, the

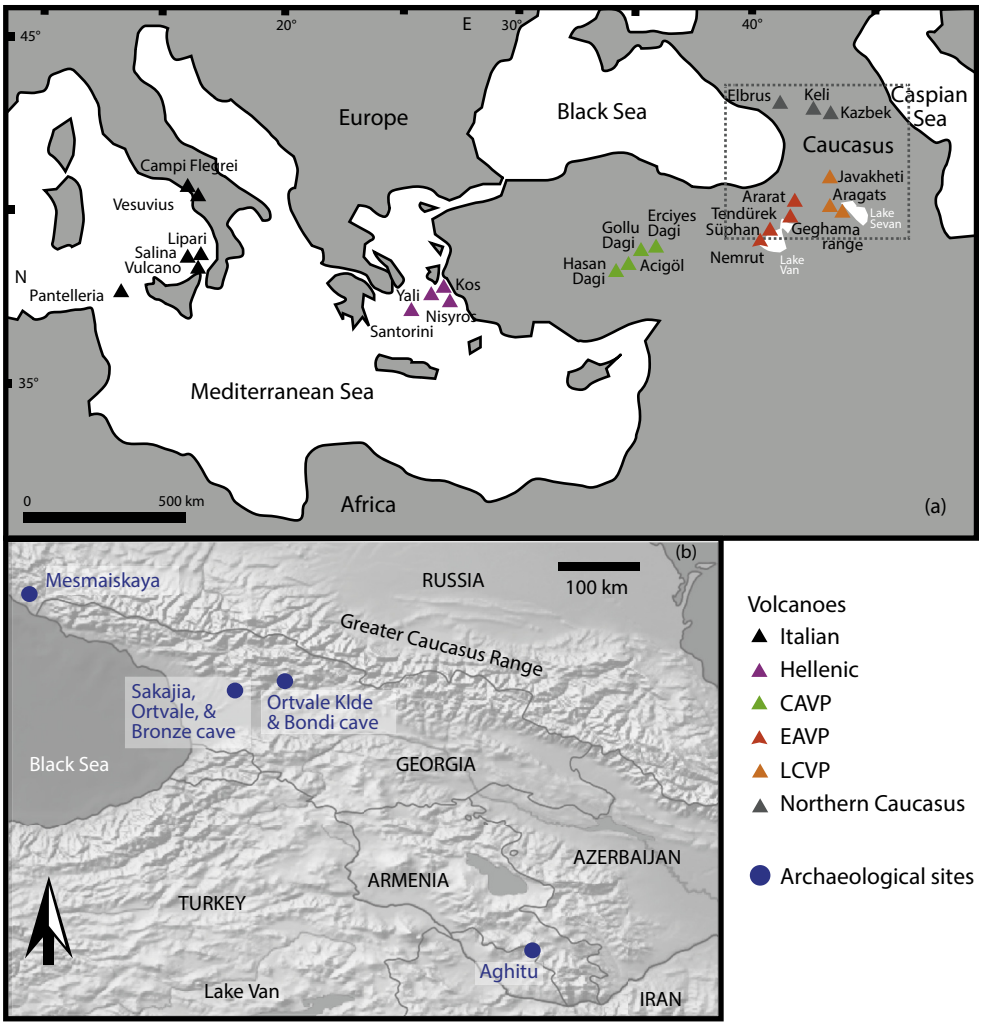

Figure 1. Map of the Caucasus region. (a) Volcanoes known to have been active in the Quaternary and those that could have deposited tephra in Ortvale Klde (triangles). The volcanoes located close to the site are part of the following volcanic regions: Italian, Hellenic, Central Anatolian Volcanic Province (CAVP), Northern Caucasus, East Anatolian Volcanic Province (EAVP), and the Lesser Caucasus Volcanic Province (LCVP). (b) The locations of archaeological sites mentioned in the text are marked with a blue circle except for Bondi Cave, which is in the same position as Ortvale Klde. (For interpretation of the references to color in this figure legend, the reader is referred to the Web version of this article.)

potential for using tephra to correlate various stratigraphic records across the region, allowing such records to be synchronized and enabling paleoenvironmental and archaeological changes to be compared (e.g., Lane et al., 2012). Furthermore, many widespread tephra associated with large eruptions have been dated using radiometric methods (e.g., indirectly using radiocarbon or directly by $^{40}Ar/^{39}Ar$), providing absolute chronologies. These tephra layers are correlated between sites on the basis of glass chemistry, given that volcanic eruptions produce geochemically distinct ejecta (e.g., Shane 2000).

Visible tephra layers were not present in the Ortvale Klde sequence, but rather cryptotephra was extracted from sediment samples (see the following paragraphs), and the glass shards were analyzed to chemically fingerprint the units for correlation. Cryptotephra typically represents the distal fallout from eruption plumes and is often found hundreds to thousands of kilometers from the source volcano. There are potential sources within the Caucasus region, for example, Elbrus, Kasbek and the Keli Highlands (Lebedev et al., 2011a, b), and the Gegham range of the Lesser Caucasus in Armenia (Karakhanian et al., 2003; Lebedev et al., 2013; Sherriff et al., 2019). Assuming Late Pleistocene global circulation patterns were the same as today, predominant winds crossing the southern Caucasus will have been westerlies, meaning that tephra from volcanic centers in Anatolia, for example, Nemrut (Sumita and Schmincke 2013a, b) and Acigöl (Mouralis et al., 2002; Tyron et al., 2009; Schmitt et al., 2011), are preserved in the region (see Fig. 1). Tephra from large eruptions in Italy and Greece might also be expected in the southern Caucasus sequences as many are widespread and found in the eastern Mediterranean Sea (Keller et al., 1978). For example, the ~39 ka Campanian Ignimbrite eruption from Campi Flegrei volcano, Italy, is the largest eruption within Europe in the last 200 ka. It dispersed ash more than 2500 km from the volcano and covered more than 3.5 million km^2 of Eastern Europe in ash (Costa et al., 2012; Smith et al., 2016). Golovanova et al. (2010a) identified a ~39 ka tephra at the LMP-EUP site of Mezmaiskaya Cave, and although the source remains unknown, they claim it caused a volcanogenic catastrophe that resulted in the extinction of local Neanderthal populations before modern human expansion into the region.

1.3. Ortvale Klde

Ortvale Klde is a karstic rock shelter comprising two east-facing chambers and is positioned ~35 m above the Cherula River near the

Table 1
Age data from Ortvale Klde used in the OxCal model.

Layer	Unit: depth (cm below datum)	Dating method	Code	Age (UnCal for ^{14}C)	Error (1σ)	Material dated	Reference for age data
2	G7: section	^{14}C	OxA23901	21,110	130	Bone (UF pretreatment)	C
3	-	^{40}Ar/^{39}Ar	NF1	29,700	4200	Single crystal	B
3	-	^{40}Ar/^{39}Ar	NF2	28,600	3000	Single crystal	B
3	-	^{40}Ar/^{39}Ar	NF3	33,700	10,900	Single crystal	B
4a	-	-	-	-	-	-	-
4b	-	-	-	-	-	-	-
4c	G8a: 278–285	^{14}C	OxA27863	39,600	1100	Bone (UF pretreatment)	C
4c	G8a: 285–291	^{14}C	OxA27931	34,650	600	Bone (UF pretreatment)	C
4c	D9-1 section: 312	^{14}C	OxA-X-2559-10[a]	41,900	1500	Bone (UF pretreatment)	C
4c	D9-1 section: 312	^{14}C	OxA-X-2352-43[a]	39,800	3100	Bone (UF pretreatment)	C
4d	G8a: 300–305/312	^{14}C	OxA27864	43,200	1700	Bone (UF pretreatment)	C
5	G7a: 304/307–315	TL	TL119	42,300	4700	Burnt flint	A
5	G7a: 315–321	TL	TL118	51,800	4700	Burnt flint	A
5	F8a: 321–333	TL	TL5	51,200	4800	Burnt flint	A
5	G8c: 326–331	TL	TL121	41,000	3700	Burnt flint	A
6	E9c: 344–352	TL	TL9	49,000	4000	Burnt flint	A
6	E9c: 344–352	TL	TL10	53,000	4600	Burnt flint	A
6	E9a: 348	TL	TL15	45,600	3500	Burnt flint	A
6	E9a: 348	TL	TL12	36,600	4000	Burnt flint	A
7	E8a: 376	ESR	OK2ESR	62,400	6200	Tooth (LU)	A
7	E8a: 401	ESR	OK3ESR	46,600	4000	Tooth (LU)	A
7	E9c: 403	ESR	OK4ESR	51,000	3800	Tooth (LU)	A
7	E9c: 404	ESR	OK5ESR	48,800	4600	Tooth (LU)	A
7	E9c: 404	ESR	OK6ESR	44,700	4200	Tooth (LU)	A
7	E8a: 376	ESR	OK2ESR	59,700	5800	Tooth (EU)	A
7	E8a: 401	ESR	OK3ESR	44,500	3600	Tooth (EU)	A
7	E9c: 403	ESR	OK4ESR	46,900	3200	Tooth (EU)	A
7	E9c: 404	ESR	OK5ESR	45,700	4100	Tooth (EU)	A
7	E9c: 404	ESR	OK6ESR	40,500	3600	Tooth (EU)	A
7	E8d: 385/392–392	TL	TL20	41,100	4500	Burnt flint	A
7	E8b: 386–392	TL	TL28	41,200	4200	Burnt flint	A
7	E8b: 386–392	TL	TL30	41,800	4500	Burnt flint	A
7	E8b: 386–392	TL	TL31	41,300	4500	Burnt flint	A
7	E8b: 386–392	TL	TL32	44,900	3800	Burnt flint	A
7	E8a: 387–392	TL	TL24	44,300	3500	Burnt flint	A
7	E8a: 387–392	TL	TL26	48,600	5100	Burnt flint	A
7	E8d: 385/392–392	TL	TL22	60,500	7400	Burnt flint	A
7	E8a: 387–392	TL	TL25	75,900	6500	Burnt flint	A

^{40}Ar/^{39}Ar = Argon-Argon dating; TL = thermoluminescence; ESR = electron spin resonance; LU = linear uptake age for ESR dated teeth; EU = early uptake age for the same sample using the ESR dating method. References: A = Adler et al. (2008); B = Sumita and Schmincke (2013a), b; C = this study.

[a] Two samples of this bone were dated. OxA-X-2352-43 had a low collagen yield, less than 1%, so the sample was processed again and gelatinized at 60 °C instead of 75 °C (OxA-X-2559-10) to increase the collagen yield. These samples were assigned OxA-X codes to highlight the break from the protocol, and these should be viewed with caution.^{14}C dates are from bone samples that underwent an ultrafiltration pretreatment (UF; ages are uncalibrated) using the protocols outlined in Brock et al. (2010). For full ages including the original^{14}C ages from Ortvale Klde see SOM and Adler et al. (2008).

town of Chiatura (Fig. 1). Excavations in the southern chamber by Tushabramishvili and Adler from 1997 to 2001 identified a LMP sequence (layer 7 to layer 5) stratigraphically below an EUP sequence, layers 4d–4a to layer 2 (Adler and Tushabramishvili, 2004) (Fig. 2). In this portion of the site, there is a stratigraphic and archaeological hiatus between the end of the LMP (layer 5) and the start of the EUP (layer 4d), the duration of which is difficult to estimate. Details of the site's stratigraphy have been published (e.g., Adler 2002; Adler and Tushabramishvili, 2004; Adler et al., 2006) and are summarized in the following paragraphs, with the addition of new taphonomic data derived from the detailed micromorphological study.

Here, the term 'LMP' is used to refer to the latest MP assemblages at Ortvale Klde, whereas the term 'EUP' is used for the earliest UP assemblages. We do not use the term 'IUP' because, even in its broadest sense, it does not accurately characterize the EUP assemblage of OK (see Kuhn and Zwyns, 2014; Kuhn, 2018). The LMP lithic assemblages were produced using the unidirectional Levallois method, and there is a predominance of elongated blanks and a variety of scraper forms. Of this LMP assemblage, 99.6% was produced from local high-quality flint, with 0.4% produced on obsidian (Adler et al., 2006). The EUP lithic and bone assemblages (layer 4d–4a to layer 2) are distinct from those of the LMP and contain unidirectional blade and bladelet cores, end scrapers on blades, rounded flake scrapers, burins, and numerous retouched bladelets and backed bladelets (Adler et al., 2006; Bar-Yosef et al., 2006). Artifacts made from local flint constitute 95% of the total EUP assemblage, whereas ~5% is made on obsidian. The nearest obsidian source is more than 100 km away (>180 km by foot), and the rise in its use during the EUP represents a statistically significant increase in the use of exotic raw materials over the LMP (Adler et al., 2006). In addition, three bevel-based bone/antler points, two polished bone/antler abraders, bone retouchers, and a single polished bone implement with a series of parallel incised lines were also found (see Adler et al., 2006; Bar-Yosef et al., 2006). Similar bone/antler tools are documented in EUP layers at the nearby cave site of Dzudzuana and at Mezmaiskaya Cave (Adler et al., 2006; Bar-Yosef et al., 2006, 2011; Golovanova et al., 2010a, b).

The chronology of Ortvale Klde is based on radiocarbon dates of human-modified bone, and charcoal, thermoluminescence (TL) dates of burnt flint artifacts, and electron spin resonance (ESR) dates of vertebrate teeth (see Adler et al., 2008 for full details). The conservative estimate for the first appearance of the EUP at the site, based on a single radiocarbon-dated bone (Adler et al., 2008), is

~44–41 ka cal BP (recalibrated age of RTT4725 in layer 4d from Adler et al., (2008) using IntCal20 and quoted at 95.4% confidence). Layer 4d did yield two additional bone dates (RTT4726 and RTT4727), which after strict discard protocols were eliminated from the final analysis based on their lack of accord with overlying and underlying layers (see Adler et al., 2008). If these three dates from layer 4d are considered together, the first appearance of the EUP would be >41 ka cal BP (recalibrated dates of RTT4725, RTT4726, and RTT4727 using IntCal20 and quoted at 95.4% confidence).

1.4. Stratigraphy

Cave and rock shelter sites are complex depositional and taphonomic settings, the varied hominin occupations of which are difficult to generalize across a site for any given time interval or layer based on the limited exposures archaeologists generally have to work with. This difficulty applies as much to the dating of any particular layer as it does to the reconstruction of hominin behaviors documented in that layer. In addition, because such behaviors can vary across space, we should expect excavations in different parts of caves and rock shelters to yield different behavioral and temporal signals. With these caveats in mind, the results reported here all stem from one particular portion of Ortvale Klde (see Fig. 4, Adler et al., 2006), the nature of which is described in detailed in the following paragraphs (Fig. 2).

From 1997 to 2001, excavations at Ortvale Klde were focused on the southern chamber, with all archaeological material excavated and recorded in 5-cm spits by quarter meter as per the natural stratigraphy of the site. Where necessary, these spits followed the contours of the layers and sublayers, beginning or terminating at the contact with an overlying or underlying layer. In this manner, tight stratigraphic control over the archaeological material was maintained within and between layers, and mixing of the material was minimized. Numerous sublayers, identified based on distinct changes in sediment matrix, texture, and/or color, were observed, but these rarely extend laterally for more than 50–100 cm and never exceed 10 cm in thickness. Because these sublayers were discontinuous, they were not typically excavated independent of the surrounding matrix or the larger lithological layers, except for the extensive sublayers identified in layer 4 (Fig. 2).

The LMP stratigraphy begins in the southern chamber of the site atop layer 11, a deposit of in situ weathered limestone that underlies all other stratigraphic layers and that sits on the limestone floor of the rock shelter (Fig. 2). Layer 7 is the oldest layer excavated between 1997 and 2001 and is rich in lithic and faunal remains; layers 10–8 are located a few meters to the north of Figure 2. The contact between layers 7 and 6 is gradational and becomes increasingly difficult to discern toward the southern part of the section. Layer 6 is composed of a black, granular matrix containing very few clasts (Fig. 2) and is very rich in lithics, fauna, ashy sediment, and charcoal. The layer is approximately 25-cm thick and bioturbated.

Layer 5 represents the latest LMP occupation and is composed of a dense accumulation of small (1–6 cm) pieces of éboulis, roughly 10–15 cm in thickness; the layer thickens to the north beyond the 1997–2001 excavations as do layers 7–6. The éboulis and finer sediments are very compact and contain high proportions of clay and abundant patinated and weathered lithic and faunal remains. These observations point to a hiatus in sedimentation, with long-term surface exposure of archaeological material. This suggests the site was not occupied continuously and may have been abandoned by LMP hominins before the appearance of the EUP. A similar situation, described in further detail in the following paragraphs, has been identified at the neighboring site of Bondi Cave where the EUP (layer V, ~40–37 ka cal BP) is separated from the underlying LMP (layer VIII and layer VII, >50 ka BP) by a rockfall deposit (layer VI, 47,500 ± 2600 BP; Tushabramishvili et al., 2012; Pleurdeau et al., 2016; Douka and Higham, 2017).

Clear stratigraphic boundaries are observed between layer 4 and layer 3 as well as between layer 3 and layer 2. The contacts between

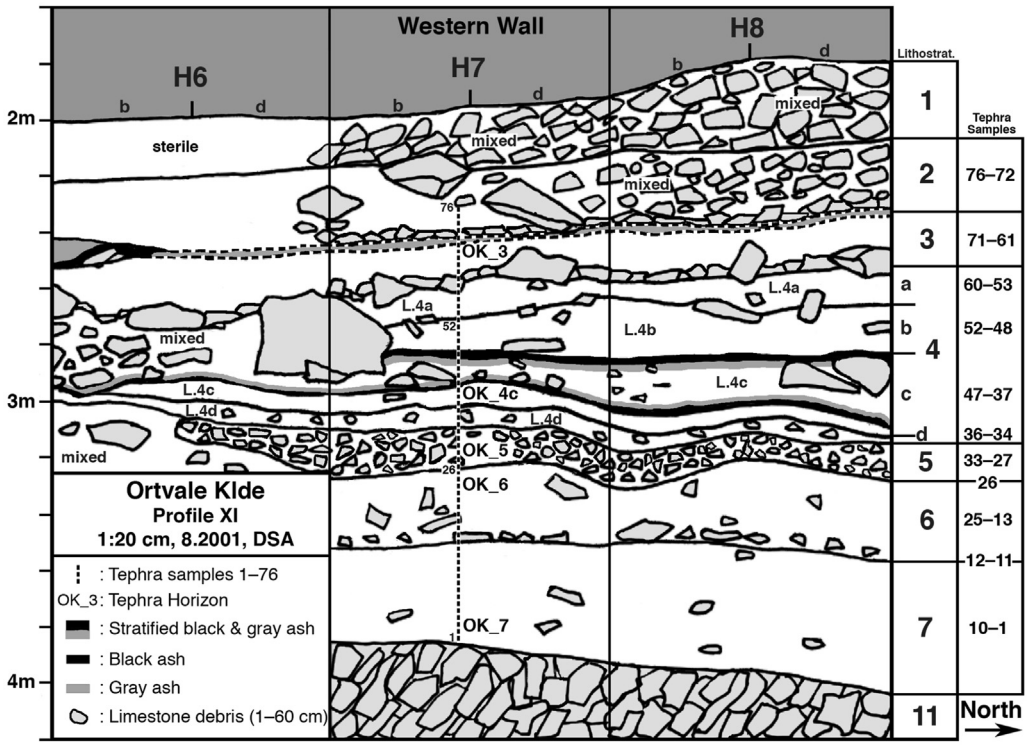

Figure 2. Profile XI with layers 11–1, sublayers 4d–4a, tephra samples 1–76, and cryptotephra horizons OK_7, OK_5/6, OK_4c, and OK_3. See Adler et al. (2008) for profile X and the location of all micromorphology samples.

these layers are defined by dense concentrations of large (~50 cm) limestone slabs and small blocks of éboulis 5–10 cm in thickness. These limestone slabs and the smaller blocks of éboulis infilling the gaps formed a barrier to sediment and artifact movement and likely represent stratigraphic unconformities of unknown duration.

Layer 4 is approximately 65cm thick, within which there are four distinct and extensive sublayers (d–a; Fig. 2). Layer 4d (EUP) is composed of a light brown, gray wood ash that fills the gaps between the dense accumulations of small limestone éboulis that cap layer 5 (LMP). Layer 4c comprises stratified gray ash and black silty lenses with charcoal, atop of which lie two finely laminated sublayers (layer 4b) and loose yellow sediment (layer 4a). The lithic and faunal assemblages found within layer 4 are ascribed to the EUP. Layer 4d also contains a hearth, ringed by large limestone blocks, which contains numerous burned microliths of flint and obsidian and dense accumulations of fine-grained dark gray ash (Adler, 2002). This feature represents the start of EUP occupation of the site and sits directly atop the weathered terminal LMP deposits of layer 5.

Lithic and faunal material is scarce in layer 3 and layer 2 relative to layer 4, with the first 10 cm of sediment in layer 3 almost completely sterile. The lithic and faunal material is concentrated near the top of the respective layers, with an extensive deposit of light gray ash found under the limestone 'platform' that divides layer 3 from layer 2 (Fig. 2) and rodent and insect burrows observed at the top of layer 3. These data likely result from ephemeral UP occupations in Marine Isotope Stage 2, when cold climatic conditions leading up to the Last Glacial Maximum prevailed across Eurasia (see Belmaker et al., 2016).

2. Materials and methods

2.1. Micromorphology

To document the taphonomic history and thus archaeological context of the dated samples reported here, we collected and analyzed five micromorphological samples at Ortvale Klde during the 2000 and 2001 field seasons. These samples were removed as oriented blocks from layer 7 to layer 1 (see Fig. 4, Adler et al., 2006) and were processed into 30-μm-thick thin sections at the Universitat de Lleida, Spain (10 × 6 cm), as well as at Spectrum Petrographics Inc., Oregon (7 × 5 cm). The thin sections were observed using a Nikon Eclipse E-POL 600 petrographic microscope under plane and cross-polarized light at 2×, 4×, 10× and 20× magnifications. Micromorphological descriptions follow standard guidelines (Stoops 2003; Courty and Goldberg, 1989).

2.2. Tephra sampling

Sampling of the Ortvale Klde sequence for tephra analysis took place in July 2010 using the same methodology outlined in Lane et al. (2014). Profile XI (Fig. 2) was cut back to expose a clean surface before sampling, after which small amounts of sediment (~10–20 g) were sampled contiguously at 2-cm resolution from the base to the top of the sequence. Samples were subsequently processed in the laboratory following the nondestructive, physical separation technique outlined in Blockley et al. (2005) and using the amendments to the procedure that are outlined by Lane et al. (2014). Thus, subsamples taken from samples across a vertical interval of 10 cm were amalgamated, and these 10-cm-resolution composites were prepared as described below. If glass shards were found in the 10-cm-resolution samples, then the remaining portion of the original 2-cm samples from the relevant interval were processed to better constrain the depth of the peak in shard concentration (i.e., the position of the isochron). The cryptotephra layers identified were labeled based on the archaeological layer in which they were preserved, for example, the cryptotephra with high glass shard concentrations in layer 4c is labeled OK_4c.

Shards from the cryptotephra layers then were manually picked and mounted on stubs for geochemical analysis (as in Lane et al., 2014). A JEOL-8600 wavelength dispersive, electron probe microanalyzer (WDS-EPMA) with four wavelength-dispersive spectrometers in the Research Laboratory for Archaeology and the History of Art, University of Oxford, was used to determine the major element composition of the individual glass shards. These shards were analyzed using a 15-keV, 6-nA, and 10-μm beam. The instrument was calibrated for 11 elements using a suite of mineral standards, and reference glasses (MPI-DING; Jochum et al., 2006) were measured alongside the samples to verify the calibration and assess precision and accuracy (see Supplementary Online Material [SOM]). These glass compositions of the cryptotephra layers in Ortvale Klde were compared with those of known eruption deposits from volcanoes in Italy, Greece, and Turkey. The glass compositions are effectively a fingerprint of a particular eruption, and correlations can be made if the major element compositions are identical (Lowe 2011). All glass chemistry data are provided in SOM. The data presented in the figures and tables have been normalized to 100% (anhydrous) for comparative purposes.

2.3. Additional faunal samples for radiocarbon dating

Twenty-six new bone samples from layer 5, layer 4d, layer 4c, layer 4b, layer 3, and layer 2 were taken for radiocarbon dating from collections (1997–2001) stored at the Georgian National Museum in Tbilisi, treated using the UF methods following the protocol outlined in Brock et al. (2010), and then analyzed by accelerator mass spectrometry at the Oxford Radiocarbon Accelerator Unit.

2.4. Age model construction

An age model for the Ortvale Klde sequence was constructed using OxCal version 4.2 (Bronk Ramsey 1995; 2009a), which used IntCal20 (Reimer et al., 2020) to calibrate the radiocarbon measurements (see SOM). Data from each layer were grouped in an OxCal 'Phase' (see SOM), with no stratigraphic order assigned to the dates within the 'Phase.' 'Boundaries' were placed within the model to mark the transitions between 'Phases,' and a double 'Boundary' was used to mark the depositional hiatus that is observed between the top of layer 5 (the end of the LMP) and layer 4d (the start of the EUP). A general outlier model (Bronk Ramsey 2009b) was used to detect and minimize the weighting of any measurements that were inconsistent with others in the sequence (Bronk Ramsey, 2009b).

3. Results

3.1. Micromorphology and taphonomy

Micromorphology samples were originally taken to examine site formation and postdepositional processes, but have proven especially useful for understanding the geological and archaeological context of the ^{14}C-dated materials and tephra. The five sediment thin sections (S.U. 1, 2, 3, 4, and 7, with the number reflecting the layer) have a broadly similar composition; they are all composed of unsorted, detrital geogenic rocks in a speckled and granostriated clayey groundmass (Fig. 3a), the latter exhibiting iron-manganese mottling throughout the sequence (Fig. 3b). The prevailing lithology consists of common subangular dolostone and fossiliferous limestone clasts ranging in size from fine sand to coarse gravel (Fig. 4). There are also minor amounts of subangular,

silt to medium sand-sized quartz grains and sand-sized glauconite grains. S.U. 7 (layer 7) contains a notably higher proportion of dolostone bedrock clasts and individual dolomite crystals in the groundmass, whereas fossiliferous limestone clasts become more numerous higher in the sequence.

Biogenic and anthropogenic components occur throughout. S.U. 7 and S.U. 4 (layer 4) contain frequent, subangular burnt and unburnt bone fragments (S.U. 7 contains higher amounts than S.U. 4; Figs. 3c and 4). Flint fragments were identified in low amounts (<5 counts in each stratigraphic unit) throughout the sequence and more frequently in S.U. 4. Charcoal was also observed, concentrating in S.U. 7 and S.U. 4 and in subrounded morphologies (Fig. 3d). Other less well-represented components include calcitic wood ash, which makes up a large proportion of the S.U. 4c groundmass, and calcitic dung spherulites, scattered throughout S.U. 1 (layer 1; Fig. 3e). S.U. 4c also shows that the two grayish black layers visible on profile XI (Fig. 2) consist of calcitic wood ash and other minute combustion residues (Fig. 5a–c).

In their microstructural aspects, most samples exhibit mosaic patterns. S.U. 7, S.U. 4, and S.U. 3 (layer 3) are dominated by granular aggregates (Fig. 6a) consisting of individual elements (rocks, bone, charcoal, or flint fragments) enveloped by clayey sediment. Some of the larger bedrock clasts are thinly coated with clay (Fig. 6b), on occasion showing microlaminated coatings (Fig. 6c). Aside from these granules, the sediment in S.U. 4, S.U. 3, and especially in S.U. 2 (layer 2) is also arranged as parallel, subhorizontal plates (Fig. 6d). In S.U. 4, the top grayish black lens of layer 4c is crumbly, whereas the bottom grayish black lens (layer 4d) preserves localized platy zones (see Fig. 5b–c). At the top of the sequence, S.U. 1 (layer 1) is angular blocky with planes, vesicles, and channels (Fig. 6e). Indeed, vesicles and channels are a common pore type throughout the sequence, as are crumbs, which are more prevalent in the lower units.

The micromorphological features reveal the existence of a local detritic deposit with a polygenetic sedimentary history marked by recurrent syndepositional human occupation, as well as recurrent postdepositional cryogenic processes and bioturbation. Based on the frequency of the anthropogenic remains, those from S.U. 7 and S.U. 4 appear to have been deposited either in situ or close to the sampled point. The presence of massive wood ash in layer 4c and layer 4d also supports the idea that anthropogenic components in the layer have not been greatly moved since original deposition. S.U. 3, S.U. 2, and S.U. 1 contain fewer anthropogenic remains, of which many are subrounded. Unfortunately, their original spatial distribution has been disturbed by postdepositional processes, which have also caused some rounding of individual elements, particularly charcoal fragments.

The entire sequence shows evidence of recurrent cryogenesis and bioturbation, suggestive of periglacial conditions throughout the formation of the sedimentary sequence. The cryogenic microstructural features identified, particularly granular aggregates and parallel referred plates, indicate recurrent seasonal freezing of the topsoil under moist conditions such as those documented in present-day periglacial contexts (Harris and Ellis, 1980; Van Vliet-Lanoe, 1982, 1985, 1998; Harris, 1987; Bertran et al., 1995; Bertran and Texier, 1999). Platy microstructures represent seasonal ice lensing, and granular aggregates are associated with gelifluction, especially in clay-rich materials (Van Vliet-Lanoe, 1976; Van Vliet-Lanoe, 1985; Van Vliet-Lanoe, 1998). Both types of feature result from mechanical stresses related to differential frost heave in clayey sedimentary contexts of diverse composition (in this case rocks, clay, bone fragments, charcoal, and organics). Such cryogenic

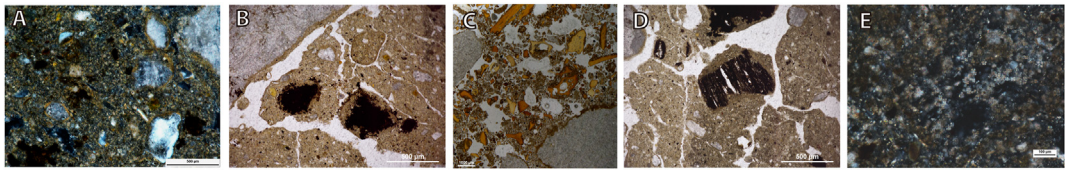

Figure 3. Characteristic micromorphological features of the Ortvale Klde sedimentary sequence: (A) detritic sand grains in a speckled and granostriated clayey groundmass; (B) parallel referred plates and localized iron-manganese mottles; (C) unsorted mix of subangular burnt and unburnt bone fragments; (D) subangular charcoal fragments; and (E) calcitic spherulites in S.U. 1.

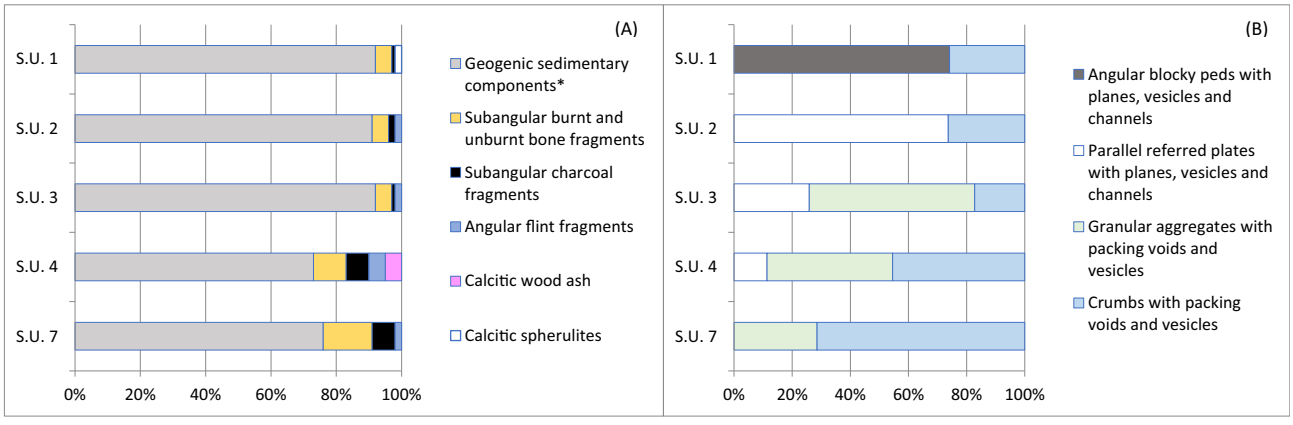

Figure 4. Micromorphological features observed throughout the Ortvale Klde sedimentary sequence and their relative proportions. A) Components; B) Microstructure and porosity types. Quantifications are approximate and were made following Stoops (2003). * The lithology of the geogenic sedimentary components is homogeneous throughout the sequence and consists of unsorted subangular, fossiliferous limestone/dolostone sand and gravel (30–50%) and subangular quartz silty sand (2–5%) in a groundmass of speckled, granostriated clay with common manganese mottles.

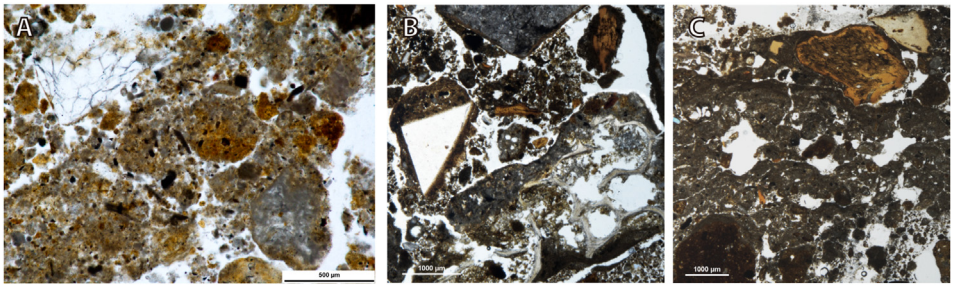

Figure 5. Evidence of anthropogenic combustion observed in the Ortvale Klde sedimentary sequence: (A) calcitic ash (light gray specks) reworked into the sedimentary matrix, (B) ashy coating on a porous bone fragment (lower right), and (C) ashy platy sediment.

processes are enhanced by high water content and high porosity (Van Vliet Lanoe, 1998). The Ortvale Klde deposits are porous owing to their sandy and gravelly composition and were possibly often water saturated, as evidenced by the ubiquitous presence of vesicles and iron-manganese mottles throughout the sequence. Cryoturbation may develop from angular blocky microstructures (such as those identified in S.U. 1) to platy and lenticular microstructures (S.U. 2, S.U. 3, and S.U. 4) and culminate with granular microstructures and clayey coatings on clasts and aggregates (S.U. 3, S.U. 4, and S.U. 7). This would suggest that S.U. 3, S.U. 4, and S.U. 7 were subject to more intense, recurrent freeze-thaw cycles than the other units (Bertran and Texier, 1999). Regarding bioturbation, it has been previously documented as a common seasonal process in periglacial contexts, where it alternates with ice lensing (Van Vliet Lanoe, 1998). At Ortvale Klde, it is indicated by the presence of crumbs and channels throughout the sequence.

Based on the micromorphological evidence, we consider it unlikely that there was any significant vertical movement of sedimentary elements, and thus the dated samples, between the different stratigraphic layers. Given the inferred periglacial context, the silt and sand-sized components were trapped within clayey aggregates, plates, or blocks as a result of cryoturbation processes operating at the surface. These processes occurred very early on as silt-sand elements and were consolidated within topsoils. Although over time, subsequent bioturbation and interstitial melting water could have released some of the finer elements, it is unlikely that these crossed major stratigraphic boundaries, as is supported by the absence of fine material in the pores, the distinct composition and microstructure of each unit (even of layer 4c and layer 4d) and the presence of roofspall deposits separating layer 2 from layer 3, layer 3 from layer 4, and layer 4 from layer 6 (Fig. 2). In sum, these observations provide strong support for the stratigraphic and contextual integrity of the archaeological materials, tephra, and dated samples found within each layer.

3.2. Tephra results from Ortvale Klde

While no visible volcanic ash layers are observed at Ortvale Klde, cryptotephra was identified within the Ortvale Klde sediment sequence (Fig. 7). These are denoted by peaks in shard concentration and are separated by sediments that do not contain glass shards, indicating that the peaks represent discrete volcanic events. The depths at which glass shards are found are (1) 164–170 cm below the datum (cm bd) in layer 7, where there is a small peak in volcanic glass shards (3 glass shards per gram of dry sediment; shards/g); (2) 112–126 cm bd, extending from the top of layer 6 (OK_6) into the base of layer 5 (OK_5, see Fig. 7a), with a peak concentration of 8 shards/g just after the boundary between the layers at 118–116 cm bd; (3) 96–98 cm bd at the contact between layer 4c and layer 4d, (208 shards/g) and 92–94 cm bd another peak slightly higher up (sample OK_4c; 238 shards/g; Fig. 7a); and (4) 30–32 cm bd in layer 3 (6 shards/g; OK_3).

The glass shards in each cryptotephra concentration are typically colorless and irregular in shape with some vesicles, cuspate features, and fluting and range in size from around 40 to 100 μm across the longest axis (Fig. 7b). There are some variations in shard morphology in some samples, with a few platy shards observed in OK_5 and some brown shards observed in OK_4c (<10%).

Only one shard in OK_7 could be geochemically analyzed, given the small size of shards and their low concentrations. The single OK_7 shard analyzed is trachy-dacitic in composition (Fig. 8) and comprises 64.71 wt.% SiO_2 (Fig. 8; Table 2; SOM). Shards from the tephra found at the top of OK_5 and base of OK_6 are compositionally similar. They are calc-alkaline rhyolites with ~75–78 wt.% SiO_2 and 4.09–5.63 wt.% K_2O and have bimodal FeOt compositions (Fig. 8).

Three compositional populations (p1, p2, and p3) are identified in the OK_4c tephra. Two of the populations are rhyolitic (p1 and p2; Table 2 and Fig. 8), and the other is dacitic (p3; Table 2 and Fig. 8). The rhyolitic populations can be differentiated from each other on total alkali concentrations, and p2 is mildly peralkaline and has higher FeOt compositions (3.08–3.28 wt.%) than those found in p1 (Fig. 8 and Table 2). The dacitic population (p3) has 61.48–68.65 wt.% SiO_2, 2.78–5.78 wt.% CaO, and 4.16–6.03 wt.% FeOt contents. This OK_4c p3 glass composition is distinct from that of all other tephras in the Ortvale Klde sequence (Fig. 8; SOM).

Glass compositions of OK_3 are rhyolitic, with two different populations (p1 and p2; Fig. 8 and Table 2). The glass chemistry in

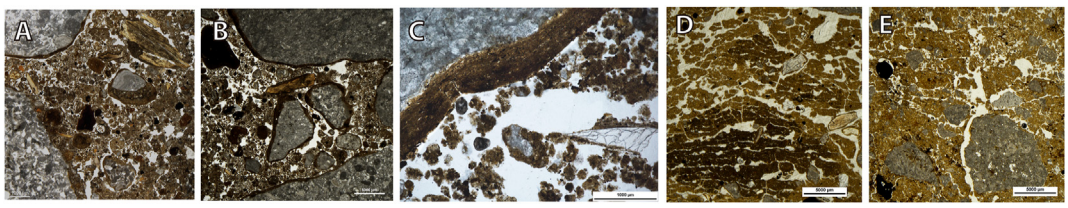

Figure 6. Cryogenic features observed throughout the Ortvale Klde sedimentary sequence: (A and B) granular aggregates and thin clay coatings, (C) microlaminated coatings (on the limestone grain, top left corner of the image), (D) parallel, subhorizontal plates, and (E) angular blocky microstructure with diffuse horizontal plates in S.U. 1.

p1 is distinct from all other volcanic glasses in the site and is characterized by elevated FeOt (~4 wt.%), while the OK_3 p2 glass shards are compositionally similar to those in OK_5/6 and OK_4c p1, with higher Al_2O_3 (>12.33 wt.%) and lower FeOt (0.39–1.29 wt.%) contents than those in OK_3 p1.

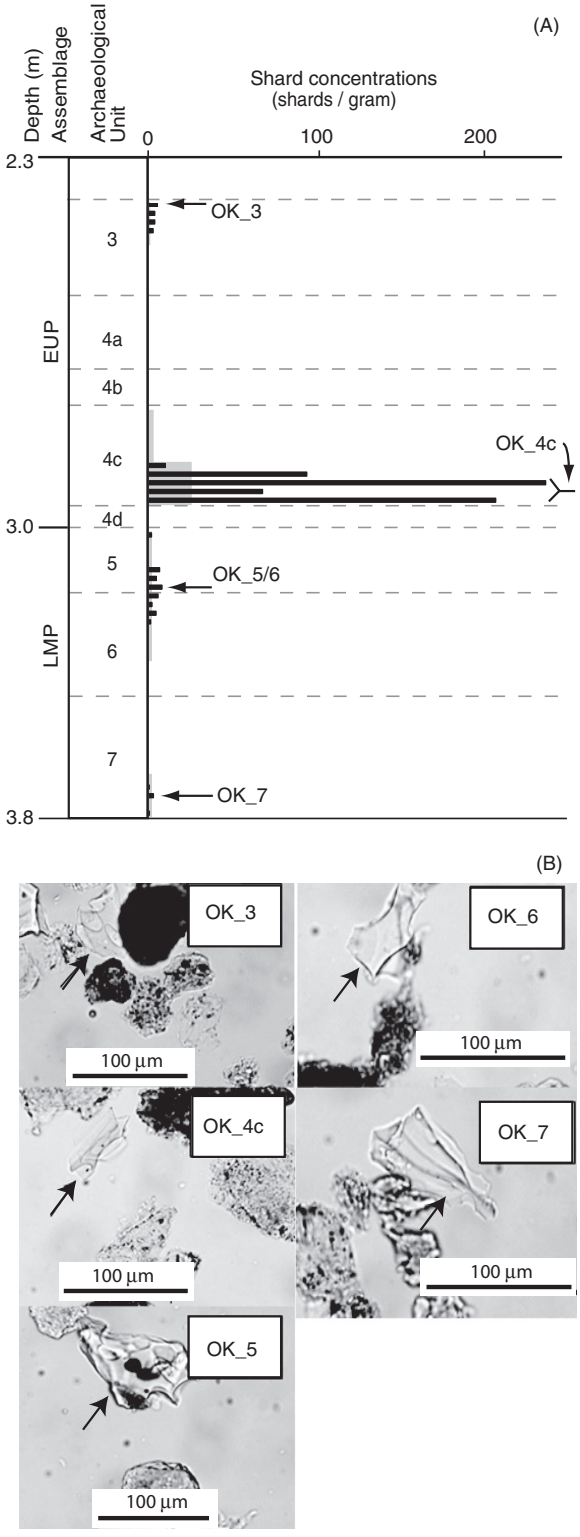

Figure 7. (A) Variation in glass shard concentrations in profile XI of Ortvale Klde, with (B) photographs of representative glass shards. Gray boxes are the shard concentrations from the initial, low-resolution samples, and the black lines are the glass shard concentrations in each of the 2-cm (high-resolution) samples. Arrows beside the tephra code (e.g., OK_3) denote the position of the isochron. EUP = Early Upper Paleolithic; LMP = Late Middle Paleolithic.

3.3. Radiocarbon ages

Only 5 of the 27 samples processed in the laboratory yielded enough collagen after pretreatment to be radiocarbon dated (Table 3). As described in Adler et al. (2006), the zooarchaeological assemblage is highly fragmented by hominins, thus limiting our ability to ascribe most bones to species. However, all bones chosen for dating exhibit evidence of hominin fracture (green breaks) rather than postdepositional breakage. One of the samples from layer 4c was dated twice, as the first measurement had a collagen yield (0.16%, 1.16 mg from a sample that weighed 727 mg; OxA-X 2352-43) that is significantly lower than that typically used for radiocarbon dates (1%). The second sample was gelatinized at 60 °C instead of 75 °C (OxA-X 2559-10) in an attempt to improve the output. Because standard Oxford Radiocarbon Accelerator Unit protocol (Brock et al., 2016) was not adhered to, the samples were assigned OxA-X numbers which imply that they should be treated with some caution. These new radiocarbon ages for samples from both layer 4d and layer 4c are at least 5 ka older than previous measurements (Adler et al., 2008, Table 3).

4. Discussion

4.1. Tephra correlations

The major element glass compositions of deposits from particular eruptions are typically unique, and volcanoes typically erupt deposits that are broadly similar (Lowe, 2011). Hence, the major element glass compositions of the cryptotephra layers in Ortvale Klde were compared with those determined for known large eruptions and particular volcanoes in the region and Eastern Europe to establish the sources of the tephra and the particular eruptions (Fig. 1). The eruption histories of most of the volcanoes in Italy and Greece (Fig. 1) are well known, and major element compositions are published for most of the eruption deposits (e.g., Tomlinson et al., 2012a, 2012b). Less is known about the eruption histories of the volcanoes in Turkey, and the glass chemistry has only been determined for some of the large eruption deposits (e.g., Tryon et al., 2009; Hamann et al., 2010), and unfortunately, very little is known about the explosive activity of volcanoes closest to Ortvale Klde (i.e., those in the Lesser Caucasus Volcanic Province [LCVP]). The lack of glass chemistry data for some of the closest volcanic sources means that it has not been possible to correlate many of the Ortvale Klde tephra at this time. Nonetheless, general compositions have allowed us to suggest likely source regions for some, and there is a cryptotephra layer preserved within the site that is from a known eruption from Turkey (Figs. 9 and 10).

The Nemrut Formation (NF) tephra was generated during a large caldera-forming eruption of Nemrut volcano in eastern Turkey (Sumita and Schmincke, 2013a, b; Fig. 1). The NF proximal deposits have been dated directly to ~30 ka using $^{40}Ar/^{39}Ar$ single crystal laser dating of anorthoclase phenocrysts (29.7 ± 4.2 ka, 33.7 ± 10.9 ka, and 28.6 ± 3.0 ka; Sumita and Schmincke, 2013a). Three eruption phases are identified in the NF deposits: the plinian fallout (lower NF) that has a peralkaline rhyolite composition; the middle NF (M-NF) pyroclastic density current (PDC) deposits that are rhyolitic to trachytic in composition; and the upper NF PDC and co-PDC deposits (U-NF) that are trachytic in composition (Sumita and Schmincke, 2013a, b).

Glass shards in OK_3 p1 are geochemically similar to those of the lower NF and M-NF units (Fig. 9) indicating that this

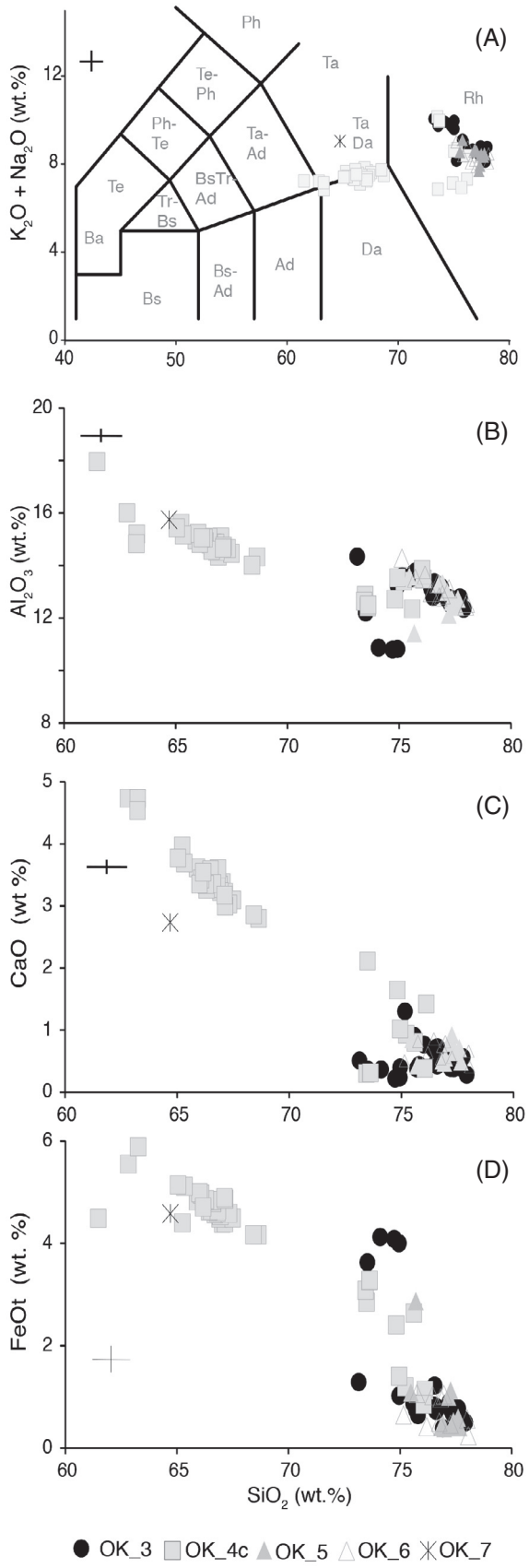

Figure 8. (A) Total alkali versus SiO_2 and (B–D) selected Harker diagrams of Ortvale Klde cryptotephra glass compositions. Both calc-alkaline and peralkaline rhyolites are found. The dacite tephra layers (OK_4c and OK_7) are clearly distinct from the other glasses in the site. Rh = rhyolite; Da = dacite; TaDa = trachydacite; Ta = trachyte; Ph = phonolite; TePh = tephri-phonolite; PhTe = phonotephrite; Te = tephrite; Ba = basanite; BS = basalt; BsAd = basaltic andesite; Ad = andesite. For full compositional glass data, see SOM Table S2.

cryptotephra is the distal equivalent of the NF. Furthermore, the modeled age estimates for the NF in Ortvale Klde (OK_3) is ~37–25 ka cal BP (see in the following paragraphs; based on the boundary transition ages for layer 4a/3 and layer 3/2), which is similar to the $^{40}Ar/^{39}Ar$ age estimates of Sumita and Schmincke (2013a,b), and additional evidence that the correlation of OK_3 to the NF is robust. This occurrence of the NF in Ortvale Klde, more than 400 km north of Nemrut (Fig. 1b), is consistent with the direction of the dispersal (Sumita and Schmincke, 2013a), thus extending the known dispersal area of tephra from this eruption and suggesting that it may be an important chronostratigraphic marker in the Caucasus region.

The rhyolitic calc-alkaline Ortvale Klde cryptotephra typically has CaO compositions <2 wt.% and FeOt compositions <1.2 wt.%, which distinguishes these deposits from known volcanic sources; for example, the Hellenic arc in Greece (e.g., Santorini) and Aeolian Islands and Pantelleria in Italy (Fig. 10A; Wulf et al., 2002; Margari et al., 2007; Asku et al., 2008; Tamburrino et al., 2012; Tomlinson et al., 2012a, b, 2014). The Ortvale Klde tephra also appears to be compositionally distinct from local volcanoes within the Caucasus although these are not particularly well studied. A deposit from Gutansar volcano, Armenia (Fig. 10), has a calc-alkaline rhyolite composition, but has higher Al_2O_3 (>14 wt%) concentrations than the Ortvale Klde glass shards.

OK_5/6 glass shards have bimodal FeOt compositions and are chemically similar to OK_3 p2 and OK_4c p1. Collectively, OK_5/6, OK_4c p1, and OK_3 p2 have similar chemical characteristics to eruption deposits from Acigöl and Gollu Dagi in the Central Anatolian Volcanic Province, Turkey (Tryon et al., 2009; Tomlinson et al., 2014, Fig. 10B), suggesting they might be deposits from these volcanoes (see Figs. 1a and 10B). Unfortunately, the limited geochemical data and low-resolution eruption chronology for the volcanoes in the region mean that we cannot yet correlate the OK_5/6, OK_4c p1, and OK_3 p2 cryptotephra layers to specific eruptions of Acigöl and Gollu Dagi.

As noted previously, tephra from OK_4c, p3 and the single glass shard analyzed from layer 7 (OK_7) are dacitic and trachy-dacitic in composition. These units typically have higher TiO_2 concentrations (>1.08 wt.%) than other well-characterized dacitic deposits, e.g., those from the Hellenic arc (Santorini; Aksu et al., 2008; Margari et al., 2007; Tomlinson et al., 2014b; see Fig. 10C) and erupted products from the Aeolian Islands (Salina; Albert et al., 2012). Volcanic provinces known to erupt dacitic compositions include the East Anatolian Volcanic Province (EAVP), Armenia (LCVP; Fig. 1), the Javakheti volcanic range in the central southern Caucasus (Lebedev et al., 2004; 2011a; Pearce et al., 1990), and Elbrus and the Keli Highlands in the northern Caucasus (Lebedev et al., 2010, 2011a, b; Chernyshev et al., 2002). Given the proximity of Ortvale Klde to these volcanoes, it is likely that they are the source of tephra. However, the tempo of explosive volcanism from these and their glass compositions is unknown, so the OK_7 and OK_4c p3 units cannot yet be correlated to a specific volcano or eruption.

The peralkaline rhyolite in OK_4c, p2, is similar in composition to the ignimbrite flow of the NF deposit (M-NF), but it is significantly older than the NF (see Tables 3–5), suggesting that it is from an earlier eruption from Nemrut. Nemrut is known to have produced a number of peralkaline trachyte and rhyolite eruptions over the last 400,000 years (e.g., AP-6/HP-10 and AP-8b; Sumita and Schmincke, 2013a, b), and some are likely to have had similar compositions (cf. Smith et al., 2011). The Tatvan Ignimbrite eruption

Table 2
Average glass shard compositions (with 1σ) of tephra layers that were identified at Ortvale Klde.

Layer_sample code	OK_3				OK_4C						OK_5		OK_6		OK_7
Population	p1	1σ	p2	1σ	p1	1σ	p2	1σ	p3	1σ	p1	1σ	p1	1σ	p1
Analysis	$n = 18$		$n = 4$		$n = 7$		$n = 3$		$n = 30$		$n = 11$		$n = 9$		$n = 1$
wt.%															
SiO_2	74.34	0.64	76.35	1.17	75.19	0.90	73.58	0.10	66.15	1.57	76.95	0.72	76.69	0.95	64.71
TiO_2	0.24	0.04	0.14	0.09	0.37	0.26	0.21	0.03	1.24	0.08	0.12	0.07	0.15	0.07	1.16
Al_2O_3	11.15	0.69	13.16	0.53	13.15	0.54	12.50	0.11	14.96	0.68	12.76	0.63	13.14	0.59	15.74
FeOt	3.96	0.23	0.81	0.23	1.78	0.82	3.21	0.11	4.78	0.42	0.85	0.73	0.70	0.31	4.58
MgO	–	–	–	–	0.44	0.42	–	–	1.40	0.26	–	–	0.10	0.06	1.31
CaO	0.28	0.08	0.54	0.24	1.18	0.58	0.30	0.01	3.55	0.62	0.63	0.16	0.65	0.16	2.72
Na_2O	5.07	0.33	3.88	0.42	4.04	0.42	5.26	0.18	4.39	0.26	3.70	0.32	3.77	0.42	5.97
K_2O	4.71	0.24	4.91	0.59	3.69	0.88	4.79	0.09	3.06	0.21	4.76	0.41	4.64	0.47	3.11
Cl	0.17	0.05	0.06	0.04	0.07	0.04	0.14	0.03	0.05	0.02	0.09	0.07	0.07	0.04	0.21

The full data set is presented in SOM Table S2.

Table 3
New ultrafiltration pretreated radiocarbon results on bone samples from Ortvale Klde.

Layer	Laboratory code	Unit: depth (cm below datum)	Material	Date ± error[a]	$\delta^{13}C$	$\delta^{15}N$	Collagen yield, %	C:N ratio	Date calibration, BP[b]
2	OxA23901	G7: section	Bone	21,110 ± 130	−18.8	+6.3	1.2	3.2	25,748–25,165
4c	OxA-X-2559-10	D9-1: section, 312[c]	Bone	41,900 ± 1500	−19.7	+5.1	1.4	3.4	48,419–42,674
4c	OxA-X-2352-43	D9-1: section, 312[c]	Bone	39,800 ± 3100	−19.7	+4.8	0.2	3.4	>40,644
4c	OxA27863	G8a: 278–285	Bone	39,600 ± 1100	−18.6	+6.8	4.5	3.2	44,905–42,115
4c	OxA27931	G8a: 285–291	Bone	34,650 ± 600	−18.5	+6.5	1.0	3.3	41,658–38,269
4d	Oxa27864	G8a: 300–305/312	Bone	43,200 ± 1700	−18.6	+5.4	2.4	3.2	51,282–43,107

[a] Uncalibrated age determinations.
[b] Ages calibrated using IntCal20 in OxCal 4.2 (Bronk Ramsey, 2009a; Reimer et al., 2020) at the 94.5% confidence level. These ages are not modeled.
[c] Two samples of this bone were dated.

occurred at ~45 ka (Sumita and Schmincke, 2013a, b), and this age is consistent with the tephra position in layer 4c (~46–36 ka cal BP; see Table 3). However, glass chemistry of a sample from the Tatvan Ignimbrite (Fig. 10) is more evolved, with lower Al_2O_3 compositions than OK_4c (p2) (>11 wt). The different glass chemistry indicates that the OK_4c p2 cryptotephra is unlikely to be associated with the

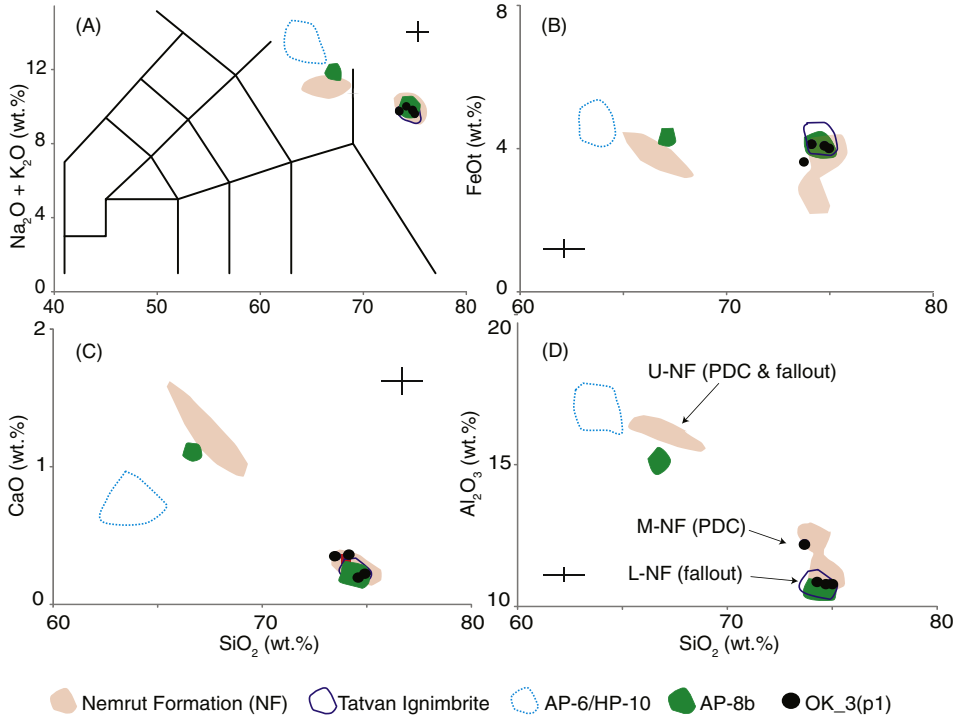

Figure 9. Major element glass compositions of OK_3 (p1) cryptotephra (black dots) compared with those of the following large eruption deposits from Nemrut volcano, Turkey: ~30 ka Nemrut Formation (NF), ~45 ka Tatvan ignimbrite, ~59 ka AP-8b, and 61 ka AP-6/HP-10 eruptions (data from Sumita and Schmincke, 2013a,b, plotted as colored fields). SiO_2 glass compositions versus (A) total alkalis ($Na_2O + K_2O$), (B) total FeO (FeOt), (C) CaO, and (D) Al_2O_3. The different eruption phases of the NF have distinct compositions, labeled on D, one of which is similar to the AP-8b tephra. The glass compositions of OK_3 (p1) plot are identical to the rhyolitic fall (L-NF) and M-NF PDC phases of the caldera-forming NF eruption, suggesting that the tephra is associated with the NF eruption. PDC = pyroclastic density current; L-NF = lower NF; M-NF = middle NF.

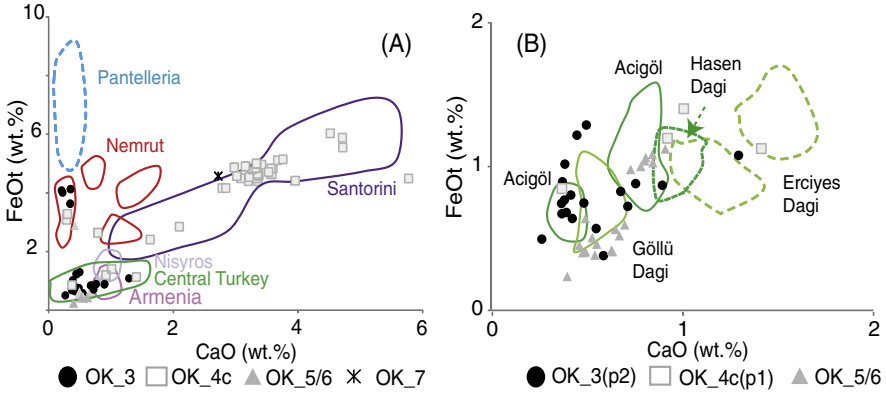

Figure 10. (A) Glass compositional data from Ortvale Klde compared with data from proximal eruption deposits (shown as colored envelopes) from various volcanoes in Figure 1, including the Cape Riva and Minoan eruption from Santorini (Wulf et al., 2002; Margari et al., 2007; Asku et al., 2008; Tomlinson et al., 2015); the Upper and Lower Pumice eruptions from Nisyros (Tomlinson et al., 2012a); Pantelleria, Italy (Tamburrino et al., 2012); Nemrut in Turkey (NF, Tatvan Ignimbrite, AP-6/HP10 and AP8b eruptions; Sumita and Schmincke, 2013a,b); and eruptions from Gutansar volcano, Armenia (see SOM). The dacitic glasses in Ortvale Klde are similar to Salina (Aeolian islands; Albert et al., 2012) and the Y2 tephra from the Cape Riva eruption of Santorini (Margari et al., 2007; Aksu et al., 2008; Tomlinson et al., 2015), but they have higher TiO_2 concentrations suggesting they do not correlate. The CAVP glass compositional data (green field) are from Hamann et al. (2010), Tryon et al. (2009), and Tomlinson et al. (2015). (B) Ortvale Klde glass compositions compared with those of eruptions from Acigöl, Hasen Dagi, Erciyes Dagi, and Göllu Dagi in the CAVP (Tryon et al., 2009; Hamann et al., 2010; Tomlinson et al., 2015). The glass compositions from Ortvale Klde are compositionally similar but do not sit within a particular field, which suggests the glass shards are probably associated with various eruptions from the CAVP. See SOM Table S2 for full compositional glass data. NF = Nemrut Formation; CAVP = Central Anatolian Volcanic Province. (For interpretation of the references to color in this figure legend, the reader is referred to the Web version of this article.)

Tatvan Ignimbrite eruption. However, it is possible it had multiple phases with different chemistry, similar to that observed in the NF deposits, and our single proximal sample is not representative of the full range of erupted chemistry. The geochemical similarity between the OK_4c p2 tephra and deposits from Nemrut volcano suggests that Nemrut is the most likely source.

4.2. Potential for using tephrochronology in the Caucasus

Our tephrochronological results suggest that a detailed and complex record of explosive activity is cryptically preserved in Late Pleistocene stratigraphic sequences in the southern Caucasus. Major element data from volcanic glass found in Ortvale Klde suggest that it records volcanic activity from the regional volcanic sources, the EAVP, possibly the CAVP, and the LCVP. Unfortunately, the limited information on past volcanism from these centers means the tephra layers cannot yet be fully exploited as absolute or relative age markers. Ages for the tephra sequence from Ortvale Klde provide a record of explosive activity from ~51–46 ka cal BP to ~32–25 ka cal BP (Table 4 and Fig. 11; model 2 boundary transitions, start layer 7 to boundary transition layer 3/2).

The identification of the ~30 ka NF tephra from Nemrut volcano in the EAVP indicates that it is widespread and probably an important chronostratigraphic marker for the region. The NF tephra is located in the Lake Van sediment cores (e.g., Stockhecke et al., 2014), detailed paleoenvironmental data of which show that the NF tephra was deposited at the end of a relatively warm and humid period (Çağatay et al., 2014), while after the ash fall, there was a high-stand in the lake level, which in turn was followed by a change to cooler and drier conditions (Çağatay et al., 2014). These changes presumably reflect the transition between Oxygen Isotope Stage 3 and Oxygen Isotope Stage 2 (unit III to unit II; Stockhecke et al., 2014). Identification of the NF in other stratigraphic records will allow a better comparison of paleoenvironmental archives and will help determine, for example, whether there was a transgression from the Black Sea to the Caspian Sea at ~30 ka (Arslanov et al., 2007; Shumilovskikh et al., 2014). Further work on proximal deposits, including geochemical characterization of the glass, and stratigraphic and chronological studies are needed for the volcanic sources in the Caucasus and Turkey. Such data will provide the chemical fingerprints required to develop a tephrostratigraphy for the region to facilitate the dating and correlation of archaeological sites and sedimentary archives.

4.3. A new Bayesian age model for the Ortvale Klde sequence

Our new Bayesian age model (model 2) diverges from the results of Adler et al. (2008) in layer 5 and layer 4 (Fig. 11). Our new radiocarbon data from samples that were prepared using the most up-to-date pretreatment procedures are more consistent than those published previously, with results from the other chronometric dating techniques used at Ortvale Klde (TL and ESR). It has been shown (Bird et al., 1999; Wood et al., 2012) that ABOx is the most reliable procedure for preparing charcoal samples >30 ka, but as the technique was not then available, the previous charcoal dates of Adler et al. (2008) for layer 4c are likely to be erroneous and are therefore excluded from our main model (model 2). The three bone samples dated from layer 4d (Adler et al., 2008), which did not undergo UF pretreatment, produced highly variable ages (41 to >50 ka cal BP). Adler et al. (2008) did not include the 45.7 ka age in their model as it was perceived an outlier after strict discard protocols. Bone dates from layer 5 (Adler et al., 2008) are also variable, ranging from 45 ka to 38 ka. Because these samples were not processed using ultrafiltration methods, these radiocarbon results have also been excluded from our main model. On the other hand, the radiocarbon data published for layer 3 and layer 2 (Adler et al., 2008) are consistent with new measurements and have been included in the model. The latter data appear to provide further evidence that the earlier pretreatment methods underestimate the ages of samples that are older than 30 ka (see Higham et al., 2009; Wood et al., 2012). To summarize, the data incorporated into the main age model for Ortvale Klde (model 2) include the following: the new UF ^{14}C ages and previously published ^{14}C ages for layer 3 and layer 2 (Adler et al., 2008); $^{39}Ar/^{40}Ar$ ages for the NF tephra in layer 3; and the ESR and TL ages from layer 7, layer 6, and layer 5 (Adler et al., 2008, Tables 1 and 5; Fig. 6).

Another three age models were produced to test the sensitivity of each model, which used different combinations of age data from the site (see Table 5). These models all produced comparable ages for the shift from the LMP to EUP at Ortvale Klde and indicate that

Table 4
Summary of the cryptotephra layers found in the archaeological layers at Ortvale Klde.[a]

Tephra	Composition	Source volcano	Proximal glass chemistry data	Age ka cal BP
OK_3 p1	PR	NF, EAVP	Sumita and Schmincke (2013 a, b)	~30 ka
OK_3 p2	CAR	Unknown (CAVP?)		Boundary transition 4a/3 ~ 37–28 ka Boundary transition 3/2 ~ 32–25 ka (Sumita and Schmincke, 2013 a, b; This study)
OK_4c p1	CAR	Unknown (CAVP?)	NA	Boundary transition 4d/4c ~46–43 ka
OK_4c p2	PR	Nemrut?		Boundary transition 4c/4b ~ 44–36 ka
OK_4c p3	D	LCVP?		(This study)
OK_5/6	CAR	Unknown (CAVP?)	NA	Boundary transition 6/5 ~48–45 ka (This study)
OK_7	TD	Unknown (LCVP?)	NA	Boundary start 7 ~51–46 ka Boundary transition 7/6 ~49–45 ka (This study)

NF = Nemrut Formation; CAR = calc-alkaline rhyolite; PR = peralkaline rhyolite; D = dacite; TD = trachy-dacite; CAVP = Central Anatolian Volcanic Province; LCVP = Lesser Caucasus Volcanic Province; EAVP = East Anatolian Volcanic Province.

[a] Ages for the identified and unknown tephras listed are taken from the chronological age of the archaeological layer in which the tephra was found (model 2). The ~$^{39}Ar/^{40}Ar$ age for the NF with the new modeled age produced in this study. Under the heading Tephra, 'p' refers to the number of compositionally distinct tephra populations found in some layers; these reflect either different source volcanoes and/or different eruptions from the same volcano. For example, the sample from layer 3 of Ortvale Klde (OK_3) contains a population of glasses with a peralkaline composition (p1) and a population that is calc-alkaline (p2; see Table 2). These populations indicate two different source volcanoes.

the EUP appeared before 44 ka cal BP. Model 2 was run using a linear uptake and early uptake model for ESR ages, with the difference between the two being ~420–180 years (95.4% confidence). Model 5 only includes published chronological data (Adler et al., 2008) and is presented for comparison (see Fig. 11, Table 5, and SOM for full details).

4.4. The LMP-EUP at Ortvale Klde and in the Caucasus

The stratigraphic, archaeological, and the age model data presented here indicate that the LMP occupation of Ortvale Klde ended ~47–44 ka cal BP. This age estimate is considerably older than that proposed for neighboring LMP-EUP sites in western Georgia using similar UF methods, for example, Sakajia, Ortvala, and Bronze caves (Adler et al., 2008; Pinhasi et al., 2012). However, these latter sites yielded relatively few datable samples (based on collagen content) on which to build a precise or accurate chronology, and moreover, no taphonomic studies (e.g., micromorphology) have been conducted to investigate site formation or postdepositional processes that might have affected the burial and disposition of the dated samples or accompanying archaeological materials. Consequently, those chronologies must be considered preliminary pending further dating and detailed taphonomic assessment. Only Bondi Cave, located ~5 km east of Ortvale Klde in the parallel valley of the Tabagrebi River, provides a roughly contemporaneous age estimate for the end of the LMP (>50 ka BP, Douka and Higham, 2017), although it too currently lacks detailed taphonomic analyses.

After the LMP at Ortvale Klde, there appears to be a hiatus in occupation (between layer 5 and layer 4d) of the southern chamber which, based on the new dates provided here, may have spanned several millennia before the appearance of the EUP at ~47–44 ka cal BP (94.5% probability; modeled boundary transition age, layer 4d; see Fig. 11 and Table 5). However, given the overlap of these two age estimates and their imprecision, the hiatus may have been of much shorter duration, but still long enough to allow for the patination of LMP artifacts in layer 5. The age estimate for the EUP at Ortvale Klde accords well with that for some sites in Eurasia, for example, ~49–45 ka cal BP and ~46–42 ka cal BP in Israel (Kebara Cave, Rebollo et al., 2011; and Manot Cave, Alex et al., 2017; respectively), ~43–35 cal ka BP in Turkey (Üçağızlı Cave, Kuhn et al., 2009), ~48–45 ka cal BP in the Altai (Denisova Cave, Douka et al., 2019), ~45 ka cal BP in Siberia (Ust'Ishim, Fu et al., 2014), ~46–43 cal ka BP in Bulgaria (Bacho Kiro, Fewlass et al., 2020), and ~47–43 cal ka BP in Italy (Grotta de Cavallo, Benazzi et al., 2011).

Neighboring archaeological sites that have been excavated with a level of precision comparable with that of Ortvale Klde include Aghitu-3 (Armenia), Bondi Cave (Georgia), and Mezmaiskaya Cave (Russia; Fig. 1), and there are broad

Table 5
Summary age data from the new Ortvale Klde Bayesian model compared with the modeled published data.

Model[a]	New ^{14}C ages[b]	TL[b]	ESR[b]	Ar^{40}/Ar^{39}[b]	Adler et al. (2008) ^{14}C ages	Boundary transition—layer 5/hiatus (end LMP), cal BP[c]	Boundary transition—hiatus/layer 4d (start EUP), cal BP[c]	Age NF tephra Boundary transition 4a/3 Boundary transition 3/2 cal BP[c]
1	◆[d]	◆	◆	◆		47,534–44284	46,845–43,754	29,752–25427/28,434–25132
2[e]	◆	◆ not layer 4c	◆	◆		47,501–44191	46,735–43,589	37,158–27614/31,633–25237
3	◆		◆	◆		50,537–44717	48,825–44,036	36,325–25938/32,345–21030
4[f]	◆			◆		78,436–44628	59,463–43,930	36,053–26078/30,597–25209
5		◆	◆		◆	44,135–41351	43,432–41,052	27,216–25741/26,136–25340

LMP = Late Middle Paleolithic; EUP = Early Upper Paleolithic; TL = thermoluminescence; ESR = electron spin resonance; LU = linear uptake.

[a] Model 1–4, this study; model 5, Adler et al. (2008).

[b] Radiocarbon (^{14}C) data are from this study; TL and ESR (LU) data are from Adler et al. (2008); $^{40}Ar/^{39}Ar$ ages are from Sumita and Schmincke (2013a, b).

[c] Age determinations are modeled ages using IntCal20 in OxCal 4.2 (Bronk Ramsey, 2009a; Reimer et al., 2020) at the 94.5% confidence level.

[d] The diamond symbol indicates what age data were used in each model.

[e] Model 2 is the preferred model used in the study.

[f] The broader age estimate for model 4 is due to a lack of age constraints below layer 4d.

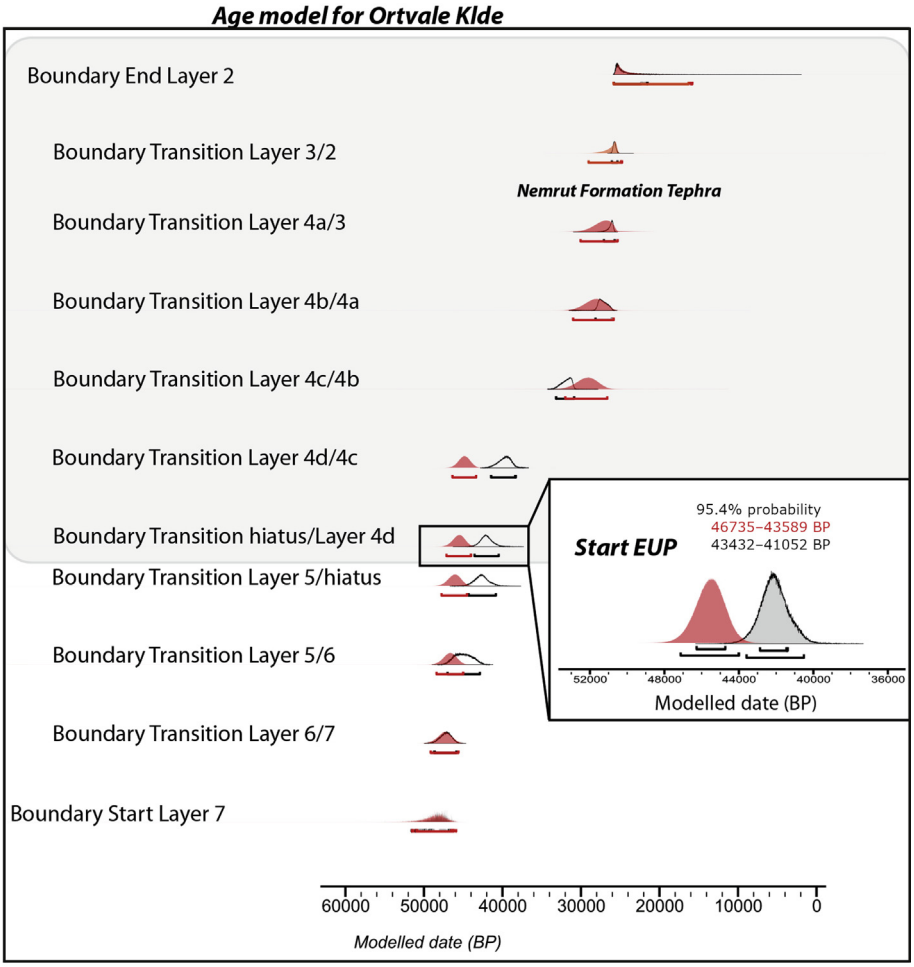

Figure 11. Bayesian age models for the Ortvale Klde sequence produced using OxCal version 4.2 (Bronk Ramsey, 2009a) and the IntCal20 calibration curve (Reimer et al., 2020). The probability distributions shown in gray are based on the original Adler et al. (2008) data (model 5, see SOM) and are presented alongside the new probability distributions (shown in red) that are based on the new chronological data presented here (model 2, see SOM). The new model dates the appearance of the EUP to ~47–44 ka cal BP (94.5% probability). See Tables 1 and 5 for information on samples and age information incorporated into both models. The actual date ranges are given at the top of the 'Start EUP' box at 95.4% probability. Ages are provided for the old remodeled data (in black) and the new modeled data (in red). Layer 7 to layer 5 = LMP; layer 4d–4a to layer 2 (grayscale) = EUP. Only the boundary between each layer is shown. EUP = Early Upper Paleolithic; LMP = Late Middle Paleolithic. (For interpretation of the references to color in this figure legend, the reader is referred to the Web version of this article.)

technotypological similarities between EUP assemblages at these sites (Bar-Yosef et al., 2006; Golovanova et al., 2010a, b; Kandel et al., 2011; 2014, 2017; Tushabramishvili et al., 2012; Pleurdeau et al., 2016). However, the chronologies of these sites indicate that the EUP appeared between roughly 10,000 and 7000 later than at Ortvale Klde (47–44 ka BP), for example, at ~39 ka cal BP in Aghitu-3 (UF ^{14}C date, see Kandel et al., 2014, 2017), ~39 ka cal BP in Mezmaiskaya Cave (conventional ^{14}C ages from layer 1C/1B; Golovanova et al., 2010b; Pinhasi et al., 2011), and ~40–37 ka cal BP at Bondi Cave (UF ^{14}C date from layer V; Douka and Higham, 2017). At Bondi Cave, layer Vb (EUP) contains a tooth (M1 dextra or M2) tentatively attributed to *H. sapiens* sp. (Tushabramishvili et al., 2012) and dated between 38.7 and 35.3 ka cal BP (95.4% probability, Douka and Higham, 2017).

The temporal gap between the LMP and EUP in the southern chamber of Ortvale Klde appears to be coeval with the rockfall deposit at Bondi Cave (layer VI, 47.5 ± 2.6 ka BP; Douka and Higham, 2017), suggesting EUP hominins may have repopulated a region already devoid of or thinly populated by LMP groups, thus allowing us to reject the hypothesis that this subregion of the southern Caucasus served as a LMP refugium. A similar pattern of regional LMP depopulation before the onset of the EUP, often correlated with Heinrich 5 and Heinrich 4, has been suggested for other sites and regions, including Bacho Kiro in Bulgaria (Fewlass et al., 2020; Hublin et al., 2020), Hohlefels in southern Germany (Conard et al., 2006; Rhodes et al., 2019), El Salt in the Iberian Peninsula (Mallol et al., 2012; Galván et al., 2014), and Mezmaiskaya in the northern Caucasus (Golovanova et al., 2010a). While future advances in AMS dating and tephra correlation may narrow this temporal gap, the pattern between sites using the same UF pretreatment protocols is consistent.

The current temporal differences in EUP occupation in the southern Caucasus suggest that simple south-to-north EUP population expansion models may not be feasible and that at a continental scale, EUP development, expansion, contraction, and interactions with LMP populations may have occurred over millennia and likely took many forms (see Greenbaum et al., 2019a,b), including but not limited to expansion into regions devoid of or lightly populated by LMP populations. Therefore, it is possible that undocumented demographic forces adversely impacted some, but not all, LMP populations across Eurasia before the arrival of EUP populations (see Abi-Rached et al., 2011; Racimo et al., 2015; Enard and Petrov, 2015; Gittelman et al., 2016; Houldcroft and Underdown, 2016).

As recently demonstrated (e.g., Slon et al., 2017; Hublin et al., 2020), the systematic application of aDNA methods is the most plausible way to test demographic hypotheses concerning the decline of the LMP and the expansion of the EUP. The routine inclusion of such methods in future archaeological excavations, or their application to existing sites, will allow the clear correlation of specific hominins (e.g., Neanderthals, *H. sapiens*, Denisovans, and so on) with specific archaeological cultures (e.g., Mousterian, EUP, IUP, 'transitional' assemblages, and so on), finally enabling meaningful discussions of the actual populations represented in any given time interval, their relationships to the archaeological record, and their expansions, interactions, and declines.

5. Conclusions

A detailed cryptotephra investigation of Ortvale Klde reveals that volcanic ash deposits from at least five eruptions are cryptically preserved across four archaeological layers. While further work is required to firmly source most of these tephra layers, the Ortvale Klde tephrostratigraphy and glass chemistry data set will facilitate future tephra correlations in the region. One cryptotephra identified in layer 3, which is ~30 ka based on associated radiocarbon determinations, has the same glass composition of the ~30 ka NF eruption from the Nemrut volcano, Turkey. This geochemical correlation extends the known dispersal of this NF eruption to ~400 km from the volcano and indicates that the tephra is a useful regional marker layer that can be used in future to correlate archaeological and paleoenvironmental sequences across the southern Caucasus. This correlation demonstrates that tephrochronology can provide age constraints for sites, and the ability for them to provide both absolute and relative chronological constraints will improve with further research into the eruption histories of volcanoes in the region.

The age of NF was integrated with new and previously published radiocarbon, TL, and ESR data in an OxCal Bayesian age model to further constrain the chronology for the Ortvale Klde sequence. These data indicate the LMP ends at ~47.5–44.2 ka cal BP (94.5% probability) and the EUP begins at ~46.7–43.6 ka cal BP (94.5% probability), which at present is the earliest evidence for the EUP in the Caucasus and among the earliest evidence for any region. These ages are broadly consistent with earlier age estimates for specific EUP sites across northern Eurasia and the Mediterranean, suggesting that the appearance of the EUP in the southern Caucasus may reflect continental demographic processes. However careful, site-by-site inspections, such as those presented here, suggest that the regional and temporal variation in technology exhibited across the LMP-EUP boundary may reflect different trajectories in local cultural evolution, interpopulation connectivity, and population expansions, contractions, and extinctions rather than a single demographic sweep across Eurasia. The potential role of regional LMP population declines before the appearance of the EUP must be investigated at other sites through the systematic application of detailed taphonomic studies. Finally, the widespread implementation of paired tephra and absolute dating programs, along with other chronometric methods, and the intersite temporal linkages such studies allow is currently among the most productive means by which to improve our inter-regional understanding of this critical time interval of human evolution.

Acknowledgments

We would like to thank coordinators and demonstrators of the short course in radiocarbon dating and Bayesian chronological analysis (members of the Oxford Radiocarbon Accelerator Unit) for the guidance in producing OxCal models. We would also like to thank M. Sumita and H.-U. Schmincke for providing proximal tephra samples from Nemrut volcano. We are grateful to R. Pinhasi for his valuable contribution and two anonymous reviewers for their thoughtful comments. Finally, we acknowledge the generous intellectual and logistical support of O. Bar-Yosef, A. Belfer-Cohen, and D. Lordkipanidze. This work was supported by a UK Natural Environment Research Council research studentship award (NE/J500045/1) to V.L.C. and grants from the Wenner-Gren Foundation for Anthropological Research (grants 6881 and 7059), the L.S.B. Leakey Foundation (https://leakeyfoundation.org), the American School of Prehistoric Research at Harvard University, and the Davis Center for Russian Studies at Harvard University to D.S.A.

Appendix A. Supplementary Online Material

Supplementary online material to this article can be found online at https://doi.org/10.1016/j.jhevol.2020.102908.

References

Abi-Rached, L., Jobin, M., Luo, M., Dalva, K., 2011. The shaping of modern human admixture with archaic humans. Science 334, 89–95.
Adler, D.S., 2002. Late Middle Palaeolithic patterns of lithic reduction, mobility, and land use in the southern Caucasus. Ph.D. Dissertation. Harvard University.
Adler, D.S., Tushabramishvili, N., 2004. Middle Palaeolithic patterns of settlement and subsistence in the Southern Caucasus. In: Conard, N.J. (Ed.), Middle Palaeolithic Settlement Dynamics. Tübingen Publications in Prehistory. Kerns Verlag, Tübingen, pp. 91–132.
Adler, D.S., Bar-Oz, G., Belfer-Cohen, A., Bar-Yosef, O., 2006. Ahead of the Game: Middle and Upper Palaeolithic Hunting Behaviors in the Southern Caucasus. Curr. Anthropol. 47, 89–118.
Adler, D.S., Bar-Yosef, O., Belfer-Cohen, A., Tushabramishvili, N., Boaretto, E., Mercier, N., Valladas, H., Rink, W.J., 2008. Dating the demise: Neanderthal extinction and the establishment of modern humans in the southern Caucasus. J. Hum. Evol. 55, 817–833.
Adler, D.S., Wilkinson, K.N., Blockley, S., Mark, D., Pinhasi, R., Schmidt-Magee, B.A., Nahapetyan, S., Mallol, C., Berna, F., Glauberman, P.J., Raczynski-Henk, Y., Wales, N., Frahm, E., Jöris, O., MacLeod, A., Smith, V., Cullen, V., Gasparyan, B., 2014. Early Levallois technology and the transition from the Lower to Middle Palaeolithic in the Southern Caucasus. Science 345, 1609–1613.
Albert, P.A., 2012. Volcanic glass geochemistry of Italian proximal deposits linked to distal archives in the Central Mediterranean region. Ph.D. Dissertation. University College London.
Alex, B., Barzilai, O., Hershkovitz, I., Marder, O., Berna, F., Caracuta, V., Abulafia, T., Davis, L., Goder-Goldberger, M., Lavi, R., Mintz, E., Regev, L., Bar-Yosef Mayer, D., Tejero, J.-M., Yeshurun, R., Ayalon, A., Bar-Matthews, M., Yasur, G., Frumkin, A., Latimer, B., Hans, M.G., Boaretto, E., 2017. Radiocarbon chronology of Manot Cave, Israel and Upper Paleolithic dispersals. Sci. Adv. 3, e1701450.
Arslanov, K.A., Dolukhanov, P.M., Gei, N.A., 2007. Climate, Black Sea levels and human settlements in Caucasus Littoral 50,000–9,000BP. Quat. Int. 167–168, 121–127.
Asku, A.E., Jenner, G., Hiscott, R.N., Isler, E.B., 2008. Occurrence, stratigraphy and geochemistry of Late Quaternary tephra layers in the Aegean Sea and the Marmara Sea. Mar. Geol. 252, 174–192.
Bard, E., Heaton, T.J., Talamo, S., Kromer, B., Reimer, R.W., Reimer, P.J., 2020. Extended dilation of the radiocarbon time scale between 40,000 and 48,000 y BP and the overlap between Neanderthals and *Homo sapiens*. Proc. Natl. Acad. Sci. U.S.A. 117, 21005–21007.
Bar-Yosef, O., Belfer-Cohen, A., Adler, D.S., 2006. The implications of the Middle-Upper Paleolithic chronological boundary in the Caucasus to Eurasian prehistory. Anthropologie XLIV 49–60.
Bar-Yosef, O., Belfer-Cohen, A., Meshveliani, T., Jakeli, N., Bar-Oz, G., Boaretto, E., Goldberg, P., Kvavadze, E., Matskevich, Z., 2011. Dzudzuana: An Upper Palaeolithic cave site in the Caucasus foothills (Georgia). Antiquity 85, 331–349.
Barton, C.M., Riel-Salvatore, J., 2012. Agents of change: modeling biocultural evolution in Upper Pleistocene western Eurasia. Adv. Complex Syst. 15 (1150003), 1–24.
Belmaker, M., Bar-Yosef, O., Belfer-Cohen, A., Meshveliani, T., Jakeli, N., 2016. The environment in the Caucasus in the Upper Paleolithic (Late Pleistocene): evidence from the small mammals from Dzudzuana Cave, Georgia. Quat. Int. 425, 4–15.
Benazzi, S., Douka, K., Fornai, C., Bauer, C.C., Kullmer, O., Svoboda, J., Pap, I., Mallegni, F., Bayle, P., Coquerelle, M., Condemi, S., Ronchitelli, A., Harvati, K., Weber, G.W., 2011. Early dispersal of modern humans in Europe and implications for Neanderthal behaviour. Nature 479, 525–528.
Bertran, P., Francou, B., Texier, J.P., 1995. Stratified slope deposits: the stone-banked sheets and lobes model. In: Slaymaker, O. (Ed.), Steepland Geomorphology. Wiley, Chichester, pp. 147–169.

Bertran, P., Texier, J.P., 1999. Facies and microfacies of slope deposits. Catena 35, 99–121.
Bird, M.I., Ayliffe, L.K., Fifield, L.K., Turney, C.S.M., Cresswell, R.G., Barrows, T.T., David, B., 1999. Radiocarbon dating of 'old' charcoal using a wet oxidation-stepped combustion procedure. Radiocarbon 41, 127–140.
Blockley, S.P.E., Pyne-O'Donnell, S.D.F., Lowe, J.J., Matthews, I.P., Stone, A., Pollard, A.M., Turney, C.S.M., Molyneux, E.G., 2005. A new and less destructive laboratory procedure for the physical separation of distal glass tephra shards from sediments. Quat. Sci. Rev. 24, 1952–1960.
Brock, F., Higham, T., Ditchfield, P., Ramsey, C.B., 2016. Current pretreatment methods for AMS radiocarbon dating at the Oxford Radiocarbon Accelerator Unit (ORAU). Radiocarbon 52, 103–112.
Bronk Ramsey, C., 1994. Analysis of chronological information and radiocarbon calibration: the Program OxCal. Archaeol. Comput. Newslett. 41, 11–16.
Bronk Ramsey, C., 1995. Radiocarbon calibration and analysis of stratigraphy: the OxCal program. Radiocarbon 37, 425–430.
Bronk Ramsey, C., 2009a. Bayesian analysis of radiocarbon dates. Radiocarbon 51, 337–360.
Bronk Ramsey, C., 2009b. Dealing with outliers and offsets in radiocarbon dating. Radiocarbon 51, 1023–1045.
Buck, C.E., Litton, C.D., Smith, A.F.M., 1992. Calibration of radiocarbon results pertaining to related archaeological events. J. Archaeol. Sci. 19, 497–512.
Çağatay, M.N., Öğretmen, N., Damci, E., Stockhecke, M., Sancar, Ü., 2014. Lake level and climate records of the last 90 ka from the Northern Basin of Lake Van, eastern Turkey. Quat. Sci. Rev. 104, 97–116.
Chernyshev, I.V., Lebedev, V.A., Bubnov, S.N., Arakelyants, M.M., Gol'tsmann, Y.V., 2002. Isotopic geochronology of Quaternary volcanic eruptions in the Greater Caucasus. Geochem. Int. 40, 1042–1055.
Clark, G.A., Riel-Salvatore, J., 2006. Observations on systematics in Paleolithic archaeology. In: Hovers, E., Kuhn, S.L. (Eds.), Transitions before the transition: evolution and stability in the Middle Paleolithic and Middle Stone Age. Plenum/Kluwer, New York, pp. 29–56.
Conard, N.J., Bolus, M., Goldberg, P., Münzel, S.C., 2006. The last Neanderthals and first modern humans in the Swabian Jura. In: Conard, N.J. (Ed.), Neanderthals and Modern Humans Meet, Tübingen Publications in Prehistory. Kerns Verlag, Tübingen, pp. 165–187.
Costa, A., Folch, A., Macedonio, G., Giaccio, B., Isaia, R., Smith, V.C., 2012. Quantifying volcanic ash dispersal and impact of the Campanian Ignimbrite super-eruption. Geophys. Res. Lett. 39 https://doi.org/10.1029/2012GL051605.
Courty, M.A., Goldberg, P. (Eds.), 1989. Soil Micromorphology in Archaeology. Cambridge University Press, Cambridge.
D'Errico, F., Stringer, C.B., 2011. Evolution, revolution or saltation scenario for the emergence of modern cultures? Phil. Trans. Roy. Soc. Lond. B Biol. Sci. 366, 1060–1069.
Douka, K., Higham, T., 2017. The chronological factor in understanding the Middle and Upper Paleolithic of Eurasia. Curr. Anthropol. 58 (Supplement 17), S480–S490.
Douka, K., Slon, V., Jacobs, Z., Bronk Ramsey, C., Shunkov, M.V., Derevianko, A.P., Mafessoni, F., Kozlikin, M.B., Li, B., Grün, R., Comeskey, D., Devièse, T., Brown, S., Viola, B., Kinsley, L., Buckley Meyer, M., Roberts, R.G., Pääbo, S., Kelso, J., Higham, T., 2019. Age estimates for hominin fossils and the onset of the Upper Palaeolithic at Denisova Cave. Nature 565, 640–644.
Enard, D., Petrov, D.A., 2015. Evidence that RNA viruses drove adaptive introgression between Neanderthals and modern humans. Cell 175, 360–371.
Fewlass, H., Talamo, S., Wacker, L., Kromer, B., Tuna, T., Fagault, Y., Bard, E., McPherron, S.P., Aldeias, V., Maria, R., Martisius, N.L., Paskulin, L., Rezek, Z., Sinet-Mathiot, V., Sirakova, S., Smith, G.M., Spasov, R., Welker, F., Sirakov, N., Tsanova, T., Hublin, J.-J., 2020. A ^{14}C chronology for the Middle to Upper Palaeolithic transition at Bacho Kiro Cave, Bulgaria. Nat. Ecol. Evol. 4, 794–801.
Flas, D., 2011. The Middle to Upper Paleolithic transition in Northern Europe: the Lincombian-Ranisian-Jerzmanowician and the issue of acculturation of the last Neanderthals. World Archaeol. 43, 605–627.
Frahm, E., Feinberg, J.M., Schmidt-Magee, B., Wilkinson, K.N., Gasparyan, B., Yeritsyan, B., Adler, D.S., 2016. Middle Palaeolithic lithic procurement behaviors at Lusakert Cave 1, Hrazdan Valley, Armenia. J. Hum. Evol. 91, 73–92.
Frahm, E., Kandel, A.W., Gasparyan, B., 2019. Upper Palaeolithic settlement and mobility in the Armenian Highlands: agent-based modeling, obsidian sourcing, and lithic analysis at Aghitu-3 Cave. J. Paleolit. Archaeol. https://doi.org/10.1007/s41982-019-00025-5.
Frahm, E., Jones, C.O., Corolla, M., Wilkinson, K.N., Gasparyan, B., Adler, D.S., 2020. Comparing Lower and Middle Palaeolithic lithic procurement behaviors within the Hrazdan basin of central Armenia. J. Archaeol. Sci. Rep. 32, 102389.
Fu, Q., Li, H., Moorjani, P., Jay, F., Slepchenko, S.M., Bondarev, A.A., Johnson, P.L.F., Aximu-Petri, A., Prufer, K., de Filippo, C., Meyer, M., Zwyns, N., Salazar-Garcia, D.C., Kuzmin, Y.V., Keates, S.G., Kosintsev, P.A., Razhev, D.I., Richards, M.P., Peristov, N.V., Lachmann, M., Douka, K., Higham, T.F.G., Slatkin, M., Hublin, J.-J., Reich, D., Kelso, J., Viola, T.B., Paabo, S., 2014. Genome sequence of a 45,000-year-old modern human from western Siberia. Nature 514, 445–449.
Fu, Q., Hajdinjak, M., Moldovan, O.T., Constantin, S., Mallick, S., Skoglund, P., Patterson, N., Rohland, N., Lazaridis, I., Nickel, B., Viola, B., Prufer, K., Meyer, M., Kelso, J., Reich, D., Pääbo, S., 2015. An early modern human from Romania with a recent Neanderthal ancestor. Nature 524, 216–219.
Galván, B., Hernández, C.M., Mallol, C., Mercier, N., Sistiaga, A., Soler, V., 2014. New evidence of early Neanderthal disappearance in the Iberian Peninsula. J. Hum. Evol. 75, 16–27.
Gamble, C., 1999. The Palaeolithic Societies of Europe. Cambridge University Press, Cambridge.
Gittelman, R.M., Schraiber, J.G., Vernot, B., Mikacenic, C., Wurfel, M.M., Akey, J.M., 2016. Archaic hominin admixture facilitated adaptation to out-of-Africa environments. Curr. Biol. 26, 3375–3382.
Golovanova, L.V., Doronichev, V.B., Cleghorn, N.E., Koulkova, M.A., Sapelko, T.V., Shackley, M.S., 2010a. Significance of ecological factors in the Middle to Upper Paleolithic Transition. Curr. Anthropol. 51, 655–688.
Golovanova, L.V., Doronichev, V.B., Cleghorn, N.E., 2010b. The emergence of bone-working and ornamental art in the Caucasian Upper Palaeolithic. Antiquity 84, 299–320.
Greenbaum, G., Getz, W.M., Rosenberg, N.A., Feldman, M.W., Hovers, E., Kolodny, O., 2019a. Disease and introgression explain the long-lasting contact zone of Modern Humans and Neanderthals and its eventual destabilization. Nat. Commun. 10, 5003. https://doi.org/10.1038/s41467-019-12862-7.
Greenbaum, G., Friesem, D.E., Hovers, E., Feldman, M.W., Kolodny, O., 2019b. Was inter-population connectivity of Neanderthals and modern humans the driver of the Upper Paleolithic transition rather than its product? Quat. Sci. Rev. 217, 316–329.
Hajdinjak, M., Fu, Q., Hübner, A., Petr, M., Mafessoni, F., Grote, S., Skoglund, P., Narasimham, V., Rougier, H., Crevecoeur, I., 2018. Reconstructing the genetic history of late Neanderthals. Nature 555, 652–656.
Hamann, Y., Wulf, S., Ersoy, O., Ehrmann, W., Aydar, E., Schmiedl, G., 2010. First evidence of a distal early Holocene ash layer in Eastern Mediterranean deep-sea sediments derived from the Anatolian volcanic province. Quat. Res. 73, 497–506.
Harris, C., Ellis, S., 1980. Micromorphology of soils in soliflucted materials, Okstindan, Northern Norway. Geoderma 23, 11–29.
Harris, C., 1987. Solifluction and related deposits in England and Wales. In: Boardman, J. (Ed.), Periglacial Processes and Landforms in Britain. Cambridge University Press, Cambridge, pp. 209–223.
Higham, T., Bronk, F., Peresani, M., Broblio, A., Wood, R., Douka, K., 2009. Problems with radiocarbon dating the Middle to Upper Palaeolithic transition in Italy. Quat. Sci. Rev. 28, 1257–1267.
Higham, T., Compton, T., Stringer, C., Jacobi, R., Shapiro, B., Trinkaus, E., Chandler, B., Groning, F., Collins, C., Hillson, S., O'Higgins, P., FitzGerald, C., Fagan, M., 2011. The earliest evidence for anatomically modern humans in north-western Europe. Nature 479, 521–524.
Higham, T., Douka, K., Wood, R., Ramsey, C.B., Brock, F., Basell, L., Camps, M., Arrizabalaga, A., Baena, J., Barroso-Ruiz, C., Bergman, C., Boitard, C., Boscato, P., Caparros, M., Conard, N.J., Draily, C., Froment, A., Galvan, B., Gambassini, P., Garcia-Moreno, A., Grimaldi, S., Haesaerts, P., Holt, B., Iriarte-Chiapusso, M.-J., Jelinek, A., Jorda Pardo, J.F., Maillo-Fernandez, J.-M., Marom, A., Maroto, J., Menendez, M., Metz, L., Morin, E., Moroni, A., Negrino, F., Panagopoulou, E., Peresani, M., Pirson, S., de la Rasilla, M., Riel-Salvatore, J., Ronchitelli, A., Santamaria, D., Semal, P., Slimak, L., Soler, J., Soler, N., Villaluenga, A., Pinhasi, R., Jacobi, R., 2014. The timing and spatiotemporal patterning of Neanderthal disappearance. Nature 512, 306–309.
Hoffecker, J.F., 2009. Out of Africa: modern human origins special feature: the spread of modern humans in Europe. Proc. Natl. Acad. Sci. U.S.A. 106, 16040–16045.
Houldcroft, C.J., Underdown, S.J., 2016. Neanderthal genomics suggests a Pleistocene time frame for the first epidemiologic transition. Am. J. Phys. Anthropol. 160, 379–388.
Hovers, E., Belfer-Cohen, A., 2006. Now you see it, now you don't"-modern human behavior in the Middle Paleolithic. In: Hovers, E., Kuhn, S.L. (Eds.), Transitions before the Transition. Springer, New York, pp. 295–304.
Hovers, E., 2009. DISCUSSION 4: The Middle-to-Upper Paleolithic transition: what news? In: Camps, M., Chauhan, P. (Eds.), Sourcebook of Paleolithic Transitions. Springer, New York, pp. 455–462.
Hublin, J.-J., 2015. The modern human colonization of western Eurasia: when and where? Quat. Sci. Rev. 118, 194–210.
Hublin, J.-J., Sirakov, N., Aldeias, V., Bailey, S., Bard, E., Delvigne, V., Endarova, E., Fagault, Y., Fewlass, H., Hajdinjak, M., Kromer, B., Krumov, I., Marreiros, J., Martisius, N.L., Paskulin, L., Sinet-Mathiot, V., Meyer, M., Pääbo, S., Popov, V., Rezek, Z., Sirakova, S., Skinner, M.M., Smith, G.M., Spasov, R., Talamo, S., Tuna, T., Wacker, T., Welker, F., 2020. Initial Upper Palaeolithic *Homo sapiens* from Bacho Kiro Cave, Bulgaria. Nature 581, 299–302.
Jacobs, Z., Li, B., Shunkov, M.V., Kozlikin, M.B., Bolikhovskaya, N.S., Agadjanian, A.K., Uliyanov, V.A., Vasiliev, S.K., O'Gorman, K., Derevianko, A.P., Roberts, R.G., 2019. Timing of archaic hominin occupation of Denisova Cave in southern Siberia. Nature 565, 594–599.
Jochum, K.P., Stoll, B., Herwig, K., Willbold, M., Hofmann, A.W., Amini, M., Aarburg, S., Abouchami, W., Hellebrand, E., Mocek, B., Raczek, I., Stracke, A., Alard, O., Bouman, C., Becker, S., Dücking, M., Brätz, H., Klemd, R., Bruin, D.d., Canil, D., Cornell, D., Hoog, C.- J.d., Dalpé, C., Danyushevsky, L., Eisenhauer, A., Gao, Y., Snow, J.E., Groschopf, N., Günther, D., Latkoczy, C., Guillong, M., Hauri, E.H., Höfer, H.E., Lahaye, Y., Horz, K., Jacob, D.E., Kasemann, S.A., Kent, A.J.R., Ludwig, T., Zack, T., Mason, P.R.D., Meixner, A., Rosner, M., Misawa, K., Nash, B.P., Pfänder, J., Premo, W.R., Sun, W.D., Tiepolo, M.,

Vannucci, R., Vennemann, T., Wayne, D., Woodhead, J.D., 2006. MPI-DING reference glasses for in situ microanalysis: new reference values for element concentrations and isotope ratios. Geochem. Geophys. 7, Q02008. https://doi.org/10.1029/2005GC001060.
Kandel, A.W., Gasparyan, B., Bruch, A.A., Weissbrod, L., Zardaryan, D., 2011. Introducing Aghitu-3, the first Upper Paleolithic cave sites in Armenia. ARAMAZD, Armen, J. Near East, Stud VI (2), 7–23.
Kandel, A.W., Gasparyan, B., Nahapetyan, S., Taller, A., Weissbrod, L., 2014. The Upper Paleolithic settlement of the Armenian Highlands. In: Otte, M., Le Brun-Ricalens (Eds.), Modes of Contacts and Mobility during the Eurasian Palaeolithic. Université de Liège, ERAUL, Liège, pp. 39–60.
Kandel, A.W., Gasparyan, B., Allué, E., Bigga, G., Bruch, A., Cullen, V.L., Frahm, E., Ghukasyan, R., Gruwier, B., Jabbour, F., Miller, C.E., Taller, A., Vardazaryan, V., Vasilyan, D., Weissbrod, L., 2017. The earliest evidence for Upper Paleolithic occupation in the Armenian Highlands at Aghitu-3 Cave. J. Hum. Evol. 110, 37–68.
Karakhanian, A., Jrbashyan, R., Trifonov, V., Philips, H., Arakelian, S., Avagyan, A., Baghdassaryan, H., Davtian, V., Ghoukassyan, Y., 2003. Volcanic hazards in the region of the Armenian nuclear power plant. J. Volcanol. Geoth. Res. 126, 31–62.
Keller, J., Ryan, W.B.F., Ninkovich, D., Altherr, R., 1978. Explosive volcanic activity in the Mediterranean over the past 200,000 years as recorded in deep-sea sediments. Geol. Soc. Am. Bull. 89, 591–604.
Kuhlwilm, M., Gronau, I., Hubisz, M.J., de Filippo, C., Prado-Martinez, J., Kircher, M., Fu, Q., Burbano, H.A., Lalueza-Fox, C., de la Rasilla, M., Rosas, A., Rudan, P., Brajkovic, D., Kucan, Z.., Gusic, I., Marques-Bonet, T., Andrés, A.M., Viola, B., Pääbo, S., Meyer, M., Siepel, A., Castellano, S., 2016. Ancient gene flow from early modern humans into Eastern Neanderthals. Nature 530, 429–433.
Kuhn, S.L., Stiner, M.C., Güleç, E., Özer, I., Yılmaz, H., Baykara, I., Açıkkol, A., Goldberg, P., Molina, K.M., Ünay, E., Suata-Alpaslan, F., 2009. The early Upper Paleolithic occupations at Üçağızlı Cave (Hatay, Turkey). J. Hum. Evol. 56, 87–113.
Kuhn, S.L., 2013. Questions of complexity and scale in explanations for cultural transitions in the Pleistocene: a case study from the early Upper Paleolithic. J. Archaeol. Method Theor. 20, 194–211.
Kuhn, S.L., Zwyns, N., 2014. Rethinking the initial Upper Paleolithic. Quat. Int. 347, 29–38.
Kuhn, S.L., 2018. An early Aurignacian arrival in southwestern Europe. Archaeol. Res. Asia 17, 2–8.
Lane, C.S., De Klerk, P., Cullen, V.L., 2012. A tephrochronology for the Late glacial palynological record of the Endinger Bruch (Vorpommern, north-east Germany). J. Quat. Sci. 27, 141–149.
Lane, C.S., Cullen, V.L., White, D., Bramham-Law, C.W.F., Smith, V.C., 2014. Cryptotephra as a dating and correlation tool in archaeology. J. Archaeol. Sci. 42, 42–50.
Lebedev, V.A., Chernyshev, I.V., Arakelyant, M.M., Gol'tsman, Y.V., Dudauri, O.Z., Vashakidze, G.T., 2004. Geochronology of the Neogene-Quaternary dacitic volcanism in the northwestern Lesser Caucasus (Georgia). Stratigr. Geol. Correl. 12, 85–101.
Lebedev, V.A., Chernyshev, I.V., Chugaev, A.V., Gol'tsman, Y.V., Bairova, E.D., 2010. Geochronology of eruptions and parental magma sources of Elbrus volcano, the Greater Caucasus: K-Ar and Sr-Nd-Pb isotope data. Geochem. Int. 48, 41–67.
Lebedev, V.A., Chernyshev, I.V., Sharkov, E.V., 2011a. Geochronological scale and evolution of Cenozoic magmatism within the Caucasian segment of the alpine belt. Dokl. Earth Sci. 441, 1656–1660.
Lebedev, V.A., Vashakidze, G.T., Arutyunyan, E.V., Yakushev, A.I., 2011b. Geochronology and evolution of quaternary volcanism at the Keli Highland, Greater Caucasus. Geochem. Int. 49, 1120–1144.
Lebedev, V.A., Chernyshev, I.V., Shatagin, K.N., Bubnov, S.N., Yakushev, A.I., 2013. The quaternary volcanic Rocks of the Geghama Highland, Lesser Caucasus, Armenia: geochronology, isotopic Sr-Nd characteristics, and origin. J. Volcanol. Seismol. 7, 204–229.
Lowe, D.J., 2011. Tephrochronology and its application: a review. Quat. Geochronol. 6, 107–153.
Lowe, J., Barton, N., Blockley, S., Ramsey, C.B., Cullen, V.L., Davies, W., Gamble, C., Grant, K., Hardiman, M., Housley, R., Lane, C.S., Lee, S., Lewis, M., MacLeod, A., Menzies, M., Müller, W., Pollard, M., Price, C., Roberts, A.P., Rohling, E.J., Satow, C., Smith, V.C., Stringer, C.B., Tomlinson, E.L., White, D., Albert, P., Arienzo, I., Barker, G., Borić, D., Carandente, A., Civetta, L., Ferrier, C., Guadelli, J.-L., Karkanas, P., Koumouzelis, M., Müller, U.C., Orsi, G., Pross, J., Rosi, M., Shalamanov-Korobar, L., Sirakov, N., Tzedakis, P.C., 2012. Volcanic ash layers illuminate the resilience of Neanderthals and early modern humans to natural hazards. Proc. Natl. Acad. Sci. U.S.A. 109, 13532–13537.
Mallol, C., Hernández, C.M., Machado, J., 2012. The significance of stratigraphic discontinuities in Iberian Middle-to-Upper Palaeolithic transitional sites. Quat. Int. 275, 4–13.
Margari, V., Pyle, D.M., Bryant, C., Gibbard, P.L., 2007. Mediterranean tephra stratigraphy revisited: results from a long terrestrial sequence on Lesvos Island, Greece. J. Volcanol. Geoth. Res. 163, 34–54.
Moncel, M.-H., Pleurdeau, D., Pinhasi, R., Yeshurun, R., Agapishvili, T., Chevalier, T., Lebourdonnec, F.-X., Poupeau, G., Nomade, S., Jennings, R., Higham, T., Tushubramishvili, N., Lordkipanidze, D., 2015. The middle palaeolithic record of Georgia: a synthesis of the technological, economic and paleoanthropological aspects. Anthropologie LIII, 93–125.
Mouralis, D., Pastre, J.-F., Kuzucuoğlu, C., Türkecan, A., Atici, Y., Slimak, L., Guillou, H., Kunesch, S., 2002. Les complexes volcaniques rhyolithiques quaternaires d'Anatolie centrale (Göllü Dag et Acigöl, Turquie): genèse, instabilité, contraintes environnementales. Quaternaire 13, 219–228.
Mussi, M., 2001. Earliest Italy: An Overview of the Italian Paleolithic and Mesolithic. Interdisciplinary Contributions to Archaeology. Kluwer Academic/Plenum Publisher, New York.
Nigst, P.R., 2012. The Early Upper Palaeolithic of the Middle Danube Region. Leiden University Press, Leiden.
Nigst, P.R., Haesaerts, P., Damblon, F., Frank-Fellner, C., Mallol, C., Götzinger, M., Niven, L., Trnka, G., Hublin, J.-J., 2014. Early modern human settlement of Europe north of the Alps occurred 43,500 years ago in a cold steppe-type environment. Proc. Natl. Acad. Sci. U.S.A. 111, 14394–14399.
Pearce, J.A., Bender, J.F., De Long, S.E., Kidd, W.S.F., Low, P.J., Güner, Y., Saroglu, F., Moorbath, S., Mitchell, J.G., 1990. Genesis of collision volcanism in eastern Anatolia, Turkey. J. Volcanol. Geoth. Res. 44, 189–229.
Peresani, M., Cristiani, E., Romandini, M., 2016. The Uluzzian technology of Grotta di Fumane and its implication for reconstructing cultural dynamics in the Middle–Upper Palaeolithic transition of Western Eurasia. J. Hum. Evol. 91, 36–56.
Pinhasi, R., Higham, T.F.G., Golovanova, L.V., Doronichev, V.B., 2011. Revised age of late Neanderthal occupation and the end of the Middle Paleolithic in the northern Caucasus. Proc. Natl. Acad. Sci. U.S.A. 108, 8611–8616.
Pinhasi, R., Nioradze, M., Tushabramishvili, N., Lordkipanidze, D., Pleurdeau, D., Moncel, M.-H., Adler, D.S., Stringer, C., Higham, T.F., 2012. New chronology for the Middle Palaeolithic of the southern Caucasus suggests early demise of Neanderthals in this region. J. Hum. Evol. 63, 770–780.
Pleurdeau, D., Moncel, M.-H., Pinhasi, R., Yeshurun, R., Higham, T., Agapishvili, T., Bokeria, M., Muskhelishvili, A., Le Bourdonnec, F.-X., Nomade, S., Poupeau, G., Bocherens, H., Frouin, M., Genty, D., Pierre, M., Pons-Branchu, E., Lordkipanidze, D., Tushabramishvili, N., 2016. Bondi Cave and the Middle-Upper Palaeolithic transition in western Georgia (south Caucasus). Quat. Sci. Rev. 146, 77–98.
Racimo, F., Sankararaman, S., Nielsen, R., Huerta-Sánchez, E., 2015. Evidence for archaic adaptive introgression in humans. Nat. Rev. Genet. 16, 359–371.
Rebollo, N.R., Weiner, S., Brock, F., Meignen, L., Goldberg, P., Belfer-Cohen, A., Bar-Yosef, O., Boaretto, E., 2011. New radiocarbon dating of the transition from the Middle to the Upper Paleolithic in Kebara Cave, Israel. J. Archaeol. Sci. 38, 2424–2433.
Reimer, P., Austin, W., Bard, E., Bayliss, A., Blackwell, P., Bronk Ramsey, C., Butzin, M., Cheng, H., Edwards, R., Friedrich, M., Grootes, P., Guilderson, T., Hajdas, I., Heaton, T., Hogg, A., Hughen, K., Kromer, B., Manning, S., Muscheler, R., Palmer, J., Pearson, C., van der Plicht, J., Reimer, R., Richards, D., Scott, E., Southon, J., Turney, C., Wacker, L., Adolphi, F., Büntgen, U., Capano, M., Fahrni, S., Fogtmann-Schulz, A., Friedrich, R., Köhler, P., Kudsk, S., Miyake, F., Olsen, J., Reinig, F., Sakamoto, M., Sookdeo, A., Talamo, S., 2020. The IntCal20 Northern Hemisphere radiocarbon age calibration curve (0–55 cal kBP). Radiocarbon 62.
Rhodes, S.E., Starkovich, B.M., Conard, N.J., 2019. Did climate determine Late Pleistocene settlement dynamics in the Ach Valley, SW Germany? PloS One 14 (5), e0215172. https://doi.org/10.1371/journal.pone.0215172.
Richter, D., Tostevin, G., Skrdla, P., 2008. Bohunician technology and thermoluminescence dating of the type locality of Brno-Bohunice (Czech Republic). J. Hum. Evol. 55, 871–885.
Ruebens, K., 2013. Regional behavior among late Neanderthal groups in Western Europe: a comparative assessment of late Middle Palaeolithic bifacial tool variability. J. Hum. Evol. 65, 341–362.
Schmitt, A.K., Danišik, M., Evans, N.J., Siebel, W., Kiemele, E., Aydin, F., Harvey, J.C., 2011. Acigöl rhyolite field, central Anatolia (part 1): high-resolution dating of eruption episodes and zircon growth rates. Contrib. Mineral. Petrol. 162, 1215–1231.
Sankararaman, S., Mallick, S., Patterson, N., Reich, D., 2016. The combined landscape of Denisovan and Neanderthal ancestry in present-day humans. Curr. Biol. 26, 1241–1247.
Shane, P., 2000. Tephrochronology: a New Zealand case study. Earth Sci. Rev. 49, 223–259.
Shea, J.J., 2006. The Middle Paleolithic of the Levant: recursion and convergence. In: Hovers, E., Kuhn, S.L. (Eds.), Transitions Before the Transition: Evolution and Stability in the Middle Paleolithic and Middle Stone Age. Plenum/Kluwer, New York, pp. 189–212.
Sherriff, J.E., Wilkinson, K.N., Adler, D.S., Arakelyan, D., Beverly, E.J., Blockley, S.P.E., Gasparyan, B., Mark, D.F., Meliksetian, K., Nahapetyan, S., Preece, K.J., Timms, R.G.O., 2019. Pleistocene volcanism and the geomorphological record of the Hrazdan Valley, Central Armenia: linking landscape dynamics and the Palaeolithic record. Quat. Sci. Rev. 226 https://doi.org/10.1016/j.quascirev.2019.105994.
Shumilovskikh, L.S., Fleitmann, D., Nowaczyk, N.R., Behling, H., Marret, F., Wegwerth, A., Arz, H.W., 2014. Orbital- and millennial-scale environmental changes between 64 and 20 ka BP recorded in Black Sea sediments. Clim. Past 10, 939–954.
Skrdla, P., 2003. Comparison of Boker Tachtit and Stránská Skála MP/UP transitional industries. J. Isr. Prehist. Soc. 33, 37–73.
Skrdla, P., 2017. Middle to Upper Paleolithic transition in Moravia: new sites, new dates, new ideas. Quat. Int. 450, 116–125.
Slon, V., Hopfe, C., Weiß, C.L., Mafessoni, F., de la Rasilla, M., Lalueza-Fox, C., Rosas, A., Soressi, M., Knul, M.V., Miller, R., Stewart, J.R., Derevianko, A.P.,

Jacobs, Z., Li, B., Roberts, R.G., Shunkov, M.V., de Lumley, H., Perrenoud, C., Gušić, I., Kućan, Ž., Rudan, P., Aximu-Petri, A., Essel, E., Nagel, S., Nickel, B., Schmidt, A., Prüfer, K., Kelso, J., Burbano, H.A., Pääbo, S., Meyer, M., 2017. Neandertal and Denisovan DNA from Pleistocene sediments. Science 356, 605–608.

Slon, V., Mafessoni, F., Vernot, B., de Filippo, C., Grote, S., Viola, B., Hajdinjak, M., Peyregne, S., Nagel, S., Brown, S., 2018. The genome of the offspring of a Neanderthal mother and a Denisovan father. Nature 561, 113–116.

Smith, V.C., Isaia, R., Pearce, N.J.G., 2011. Tephrostratigraphy and glass compositions of post-15 kyr Campi Flegrei eruptions: implications for eruption history and chronostratigraphic markers. Quat. Sci. Rev. 30, 3638–3660.

Smith, V.C., Isaia, R., Engwell, S.L., Albert, P.G., 2016. Tephra dispersal during the Campanian Ignimbrite (Italy) eruption: implications for ultra-distal ash transport during the large caldera-forming eruption. Bull. Volcanol. 78, 45. https://doi.org/10.1007/s00445-016-1037-0.

Stockhecke, M., Kwiecien, O., Vigliotti, L., Anselmetti, F.S., Beer, J., Çağatay, M.N., Channell, J.E.T., Kipfer, R., Lachner, J., Litt, T., Pickarski, N., Sturm, M., 2014. Chronostratigraphy of the 600,000 year old continental record of Lake Van (Turkey). Quat. Sci. Rev. 104, 8–17.

Stoops, G., 2003. Guidelines for Analysis and Description of Soil and Regolith Thin Sections. Soil Science Society of America, Madison, WI.

Stutz, A.J., Shea, J.J., Rech, J.A., Pigati, J.S., Wilson, J., Belmaker, M., Albert, R.M., Arpin, T., Cabanes, D., Clark, J.L., 2015. Early Upper Paleolithic chronology in the Levant: new ABOx-SC accelerator mass spectrometry results from the Mughr el-Hamamah Site, Jordan. J. Hum. Evol. 85, 157–173.

Sumita, M., Schmincke, H.-U., 2013a. Impact of volcanism on the evolution of Lake Van I: evolution of explosive volcanism of Nemrut Volcano (eastern Anatolia) during the past >400,000 years. Bull. Volcanol. 75, 714.

Sumita, M., Schmincke, H.-U., 2013b. Impact of volcanism on the evolution of Lake Van II: temporal evolution of explosive volcanism of Nemrut Volcano (eastern Anatolia) during the past ca. 0.4 Ma. J. Volcanol. Geoth. Res. 253, 15–34.

Tamburrino, S., Insinga, D.D., Sprovieri, M., Petrosino, P., Tiepolo, M., 2012. Major and trace element characterization of tephra layers offshore Pantelleria Island: insights into the last 200 ka of volcanic activity and contribution to the Mediterranean tephrochronology. J. Quat. Sci. 27, 129–140.

Teyssandier, N., 2008. Revolution or evolution: the emergence of the Upper Paleolithic in Europe. World Archaeol. 40, 493–519.

Tomlinson, E.L., Kinvig, H.S., Smith, V.C., Blundy, J.D., Gottsmann, J., Müller, W., Menzies, M.A., 2012a. The Upper and Lower Nisyros Pumices: Revisions to the Mediterranean tephrostratigraphic record based on micro-beam glass geochemistry. J. Volcanol. Geoth. Res. 243–244, 69–80.

Tomlinson, E.L., Arienzo, I., Civetta, L., Wulf, S., Smith, V.C., Hardiman, M., Lane, C.S., Carandente, A., Orsi, G., Rosi, M., Müller, W., Menzies, M.A., 2012b. Geochemistry of the Phlegraean Fields (Italy) proximal sources for major Mediterranean tephras: implications for the dispersal of Plinian and co-ignimbritic components of explosive eruptions. Geochem. Cosmochim. Acta 93, 102–128.

Tomlinson, E.L., Albert, P.G., Wulf, S., Brown, R.J., Smith, V.C., Keller, J., Orsi, G., Bourne, A.J., Menzies, M.A., 2014. Age and geochemistry of tephra layers from Ischia, Italy: constraints from proximal-distal correlations with Lago Grande di Monticchio. J. Volcanol. Geoth. Res. 287, 22–39.

Tomlinson, E.L., Smith, V.C., Albert, P.G., Aydar, E., Civetta, L., Cioni, R., Çubukçu, E., Gertisser, R., Isaia, R., Menzies, M.A., Orsi, G., Rosi, M., Zanchetta, G., 2015. The major and trace element glass compositions of the productive Mediterranean volcanic sources: tools for correlating distal tephra layers in and around Europe. Quat. Sci. Rev. 118, 48–66.

Tostevin, G.B., 2000. The Middle to Upper Paleoltihic transition from the Levant to Central Europe: in situ development or diffusion? In: Orschiedt, J., Weniger, G.-C. (Eds.), Neanderthals and Modern Humans: Discussing the Transition. Neanderthal Museum, Mettmann, pp. 92–111.

Tostevin, G.B., 2012. Seeing Lithics: A Middle-range Theory for Testing for Cultural Transmission in the Pleistocene. American School of Prehistoric Research Monograph Series, Peabody Museum, Harvard University and Oxbow Books.

Tushabramishvili, N., Pleurdeau, D., Moncel, M.-H., Agapishvili, T., Vekua, A., Bukhsianidze, M., Maureille, B., Muskhelishvili, A., Mshvildadze, M., Kapanadze, N., Lordkipanidze, D., 2012. Humanremains from a new Upper Pleistocene sequence in Bondi Cave (Western Georgia). J. Hum. Evol. 62, 179–185.

Tryon, C.A., Logan, M.A.V., Mouralis, D., Kuhn, S., Slimak, L., Balkan-Atli, N., 2009. Building a tephrostratigraphic framework for the Paleolithic of Central Anatolia, Turkey. J. Archaeol. Sci. 36, 637–652.

Van Vliet-Lanoe, B., 1976. Traces de glace de ségrégation en lentilles associées aux sols et phénomènes périglaciaires fossiles. Biul. Peryglac. 26, 41–55.

Van Vliet-Lanoe, B., 1982. Structures et microstructures associées à la formation de glace de ségrégation: leurs conséquences. In: Proceedings of the 4th International Conference on Permafrost, Fairbanks, AK, pp. 116–122.

Van Vliet-Lanoe, B., 1985. Frost effects in soils. In: Boardman, J. (Ed.), Soils and Quaternary Landscape Evolution. John Wiley and Sons, Chichester, pp. 117–158.

Van Vliet-Lanoe, B., 1998. Frost and soils. Implications for paleosols, paleoclimates and stratigraphy. Catena 34, 157–183.

Vernot, B., Tucci, S., Kelso, J., Schraiber, J.G., Wolf, A.B., Gittelman, R.M., Dannemann, M., Grote, S., McCoy, R.C., Norton, H., 2016. Excavating Neandertal and Denisovan DNA from the genomes of Melanesian individuals. Science 352, 235–239.

Villa, P., Roebroeks, W., 2014. Neanderthal demise: an archaeological analysis of the modern human superiority complex. PloS One 9 (4), e96424. https://doi.org/10.1371/journal.pone.0096424.

Wood, R.E., Douka, K., Boscato, P., Haesaerts, P., Sinitsyn, A., Higham, T.F.G., 2012. Testing the ABOx-Sc method: dating known-age charcoals associated with the Campanian Ignimbrite. Quat. Geochronol. 9, 16–26.

Wulf, S., Kraml, M., Kuhn, T., Schwarz, M., Inthorn, M., Keller, J., Kuscu, I., Halbach, P., 2002. Marine tephra from the Cape Riva eruption (22 ka) of Santorini in the Sea of Marmara. Mar. Geol. 183, 131–141.

Wynn, T., Overmann, K.A., Coolidge, F.L., 2016. The false dichotomy: a refutation of the Neandertal indistinguishability claim. J. Anthropol. Sci. 94, 201–221.

Yang, M.A., Gao, X., Theunert, C., Tong, H., Aximu-Petri, A., Nickel, B., Slatkin, M., Meyer, M., Pääbo, S., Kelso, J., 2017. 40,000-year-old individual from Asia provides insight into early population structure in Eurasia. Curr. Biol. 27, 3202–3208.